Presentation on Dissertation Work Phase-2

DESIGN AND DEVELOPMENT OF SERIES RESONANT CONVERTER FOR UPS BATTERY CHARGING APPLICATION

by
Shubham Borkar
(20GAEL3011)

Under the guidance of
Dr. K. P. Guruswamy
Associate Professor

Department of Electrical and Electronics Engineering,
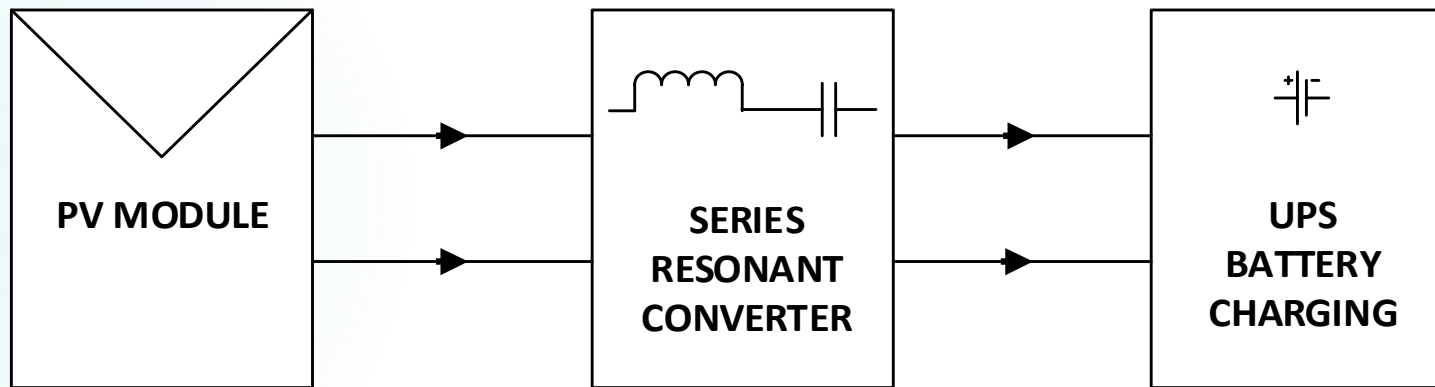**UVCE, K. R. Circle, Bengaluru- 560001**

30-03-2023

1

Contents

2

1. INTRODUCTION

- The utilization of series-resonant DC-DC converters operation at frequencies higher than the resonant frequency provides a number of advantages.

- The resonant tank circuit and the load connected at the output of the rectifier are in series.

Fig 1: Block diagram for Proposed Series Resonant Converter [1]

- **The half-bridge inverter consists of two switches including its body diode and parasitic capacitors.**

- **The SRC acts as a voltage divider circuit.**

- **The SRC converter includes a capacitor on the primary side of the transformer that will block the block dc component of primary current**

- **The SRC includes a half-bridge inverter, two element resonant network, isolation transformer and rectifier**
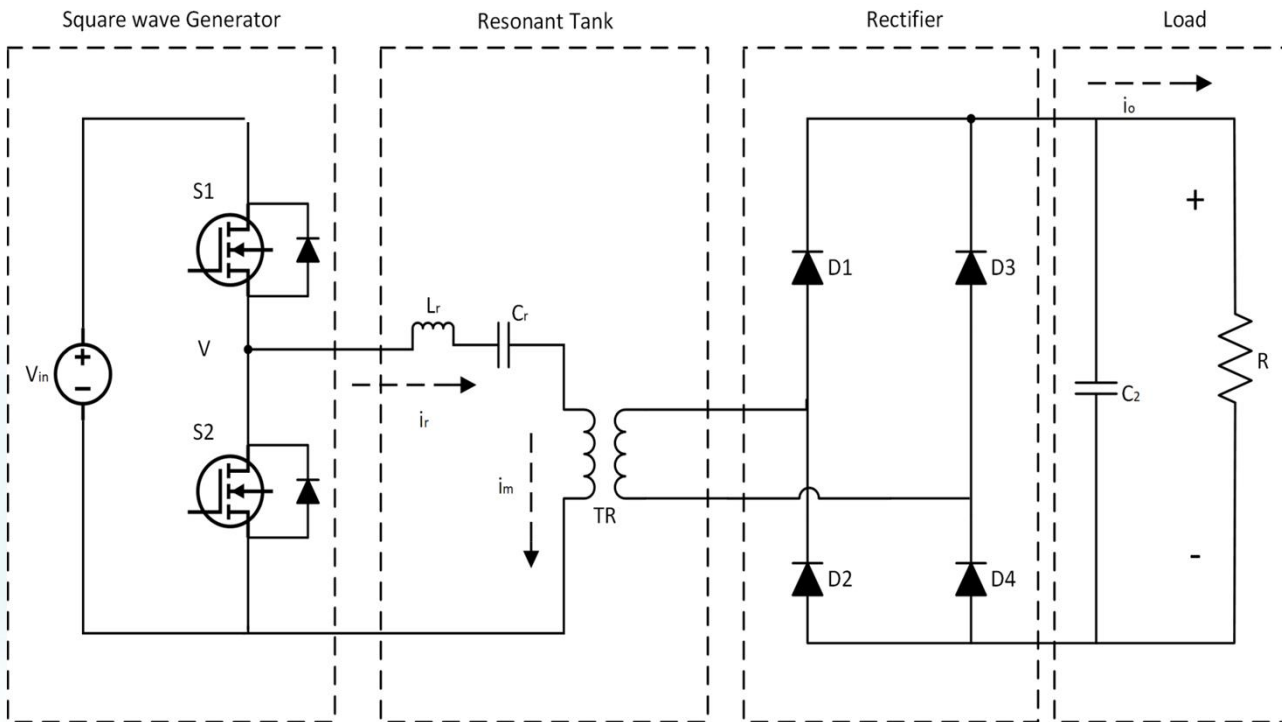
Fig 2: Circuit diagram of Series Resonant Converter (SRC) [6]

30-03-2023
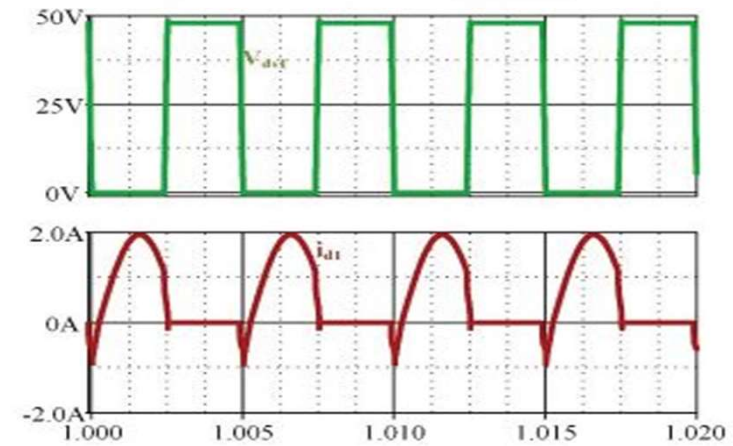
Fig 3: Voltage and currents of switch S1

Fig 4: Voltage and currents of switch S2

2. LITERATURE SURVEY

Literature Survey on various DC-DC converters.

Table 1: Comparison Table for Different Converters.

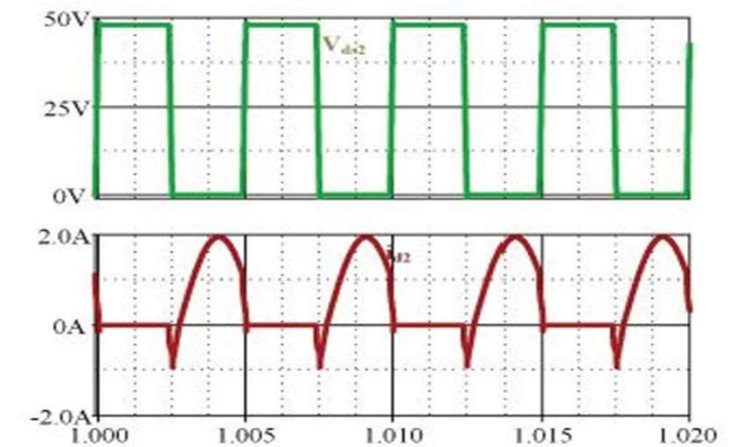| Proposed Converter	Controller	Efficiency	No. of Diodes	No. of Switches	Applications	Source	Software	Advantages	Disadvantages
Buck	PI Controller	95%	1	5	Dual mode or Standalone application	PV	Matlab	Stable fixed frequency.	Error amplifier compensation.
Boost	PI Controller	99%	3	6	3 phase inverter	PV	Matlab	Reduced ripple voltage	Higher core losses.
Sepic	Voltage mode control	99.43%	1	2	Used in both resistive and battery loads	PV	Matlab	Fast tracking, less complexity	Drift problem occurs.
Cuk	PI Controller	98.9%	1	2	Generate error signals	PV	Matlab	Feasibility and improved functionality	nonlinearity nature of PV

Table 2: Comparison Table for Different Control Technique.

Controller	Proposed Converter	Efficiency	No. of Diodes	No. of Switches	Applications	Source	Software	Advantages	Disadvantages
Fuzzy logic control	Boost	---	1	2	Mobile, transportation,	PV	Matlab	Improved reliability, better economics	high fabrication cost, low conversion efficiency
Sliding mode control	Boost	High	1	2	satellite systems.	PV	Matlab	Better voltage regulation.	No limits on control cost
Predictive control	Boost	High	2	3	voltage regulator module	PV	Matlab	High switching frequency	P&O is relatively slow
Current mode control	Buck	90%	1	3	Li-ion battery, battery charging	PV	Matlab	High speed ADC	This method does not employ true MPP detection
Voltage mode control	Boost	High	1	2	Low power application	PV	Matlab	High dynamic and static efficiencies	Required loop compensation
PI control	Boost	99.98%	2	3	High speed MPPT module	PV	Matlab	High accuracy, high efficiency	Drift problem occurs.

Table 3: Comparison Table for Different MPPT Techniques.

MPPT techniques	Converter	Controller	Efficiency	No. of Diodes	No. of Switches	Application	Source	Software	Advantage	disadvantage
Perturbation and Observation	Boost	PI Controller	96%	4	5	Fuel cell stack, battery	PV	---	High voltage gain	Increased complexity
Incremental Conductance	Boost	Predictive control	High	1	2	Generating the error signal	PV	Matlab	Very quickly MPP	Heavy oscillations problems.
Proposed MPPT	Boost	---	Medium	1	2	Residential	PV	Matlab	Low maintenance cost	Slow to respond
Ripple Correlation	Buck	PI Controller	99.30%	---	2	Mobile application	PV	PLECS		reduced tracking efficiency

Literature survey on Resonant converters

Table 4: Comparison Table for Different Resonant converters.

Proposed Converter	Controller	Efficiency	No. of Diodes	No. of Switches	Applications	Source	Software	Advantages	Disadvantages
Series resonant converter	Average Geometric Control	95%	4	8	battery packs, hybrid automobiles and photovoltaic systems	PV	Matlab	AGC controller has ability to prevent voltage overshoot following disturbances	Limited frequency and high switching losses
LLC resonant converter	Adaptive Voltage Control	High	2	4	off-line applications where hold-up time is normally required	PV	Matlab	Reduced ripple voltage	Difficulty in achieving consistent dynamic performance
LCC resonant converter	Current mode control	---	2	6	Integrated circuits	PV	Matlab	Able to achieve wide operation together with high efficiency	Carry higher peak current values

30-03-2023

Literature survey on Series Resonant Converter

Table 5: Comparison Table for Series Resonant Converters.

Paper	Controller	Efficiency	No. of Diodes	No. of Switches	Applications	Source	Software	Advantages	Disadvantages
[1]	Hybrid Controller	Higher	8	12	Industrial magnetron, renewable energy, LED driver.	DC supply	Matlab	Higher power density, lower electromagnetic interference.	Complex circuit and high cost.
[2]	Linear PI Controller	---	4	8	power factor corrector systems	DC supply	PSIM	prevent voltage overshoot following disturbances	large transients
[3]	PI controller	Higher	8	8	bidirectional power flow applications	DC supply	Matlab	greater efficiency for light loads	Switching frequency is not constant
[4]	---	95.6%	6	10	battery charging and constant power motor drive	DC supply	Matlab	the switches are soft commutated	high component count, increased cost and complexity
[5]	volatge/ current stabilization controller	96.15%	8	16	high-voltage low-current applications	DC supply	PSIM	high power density, high efficiency and soft switching	high circulation current at light load

Paper	Controller	Efficiency	No. of Diodes	No. of Switches	Applications	Source	Software	Advantages	Disadvantages
[6]	PI controller	96%	6	10	3 – phase inverter	DC supply	Matlab	Stable fixed frequency.	Error amplifier compensation
[7]	Fuzzy logic controller	97%	4	6	Used in both resistive and battery loads	DC supply	PSIM	Fast tracking, less complexity	Drift problem occurs.
[8]	Sliding mode control	---	8	8	satellite systems.	DC supply	PSIM	Better voltage regulation.	No limits on control cost
[9]	Voltage mode control	---	6	10	Low power application	DC supply	Matlab	High dynamic and static efficiencies	Required loop compensation
[10]	PI controller	Higher	8	12	Fuel cell stack, battery	DC supply	PSIM	High voltage gain	Increased complexity

30-03-2023

3. PROBLEM STATEMENT

1. The switching frequency of a non-isolated dc-dc converter are less so they cannot operate at high switching frequency.

2. In LLC and LCC resonant converter the weight and size of the converter is increased and also the complexity.

3. SRC cannot operate at no-load condition is one of the limitations of the SRC converter.

4. SRC is not suitable for low-voltage high current applications

4. OBJECTIVES

1. **To study and analyze the performance of the series resonant converter.**

2. **To understand the modeling and design of the series resonant converter for UPS battery charging application.**

3. **To understand and perform the simulation of series resonant converter in open loop system in order to validate the theoretical design.**

4. **To design the controller for the series resonant converter for UPS battery charging application.**

5. **To understand and perform the simulation of series resonant converter in closed loop system .**

30-03-2023

5. METHODOLOGY

1. The topic of the dissertation work selected will be based on its serviceability in the society.

2. The problem statement will be defined by obtaining information by referring to various literature(s) related to the topic selected.

3. The analysis will be done on the existing technology.

4. The Series Resonant Converter (SRC) will be designed for UPS battery charging applications.

5. Software Simulation for the same will be performed using MATLAB.

6. ANALYSIS OF SERIES RESONANT CONVERTER
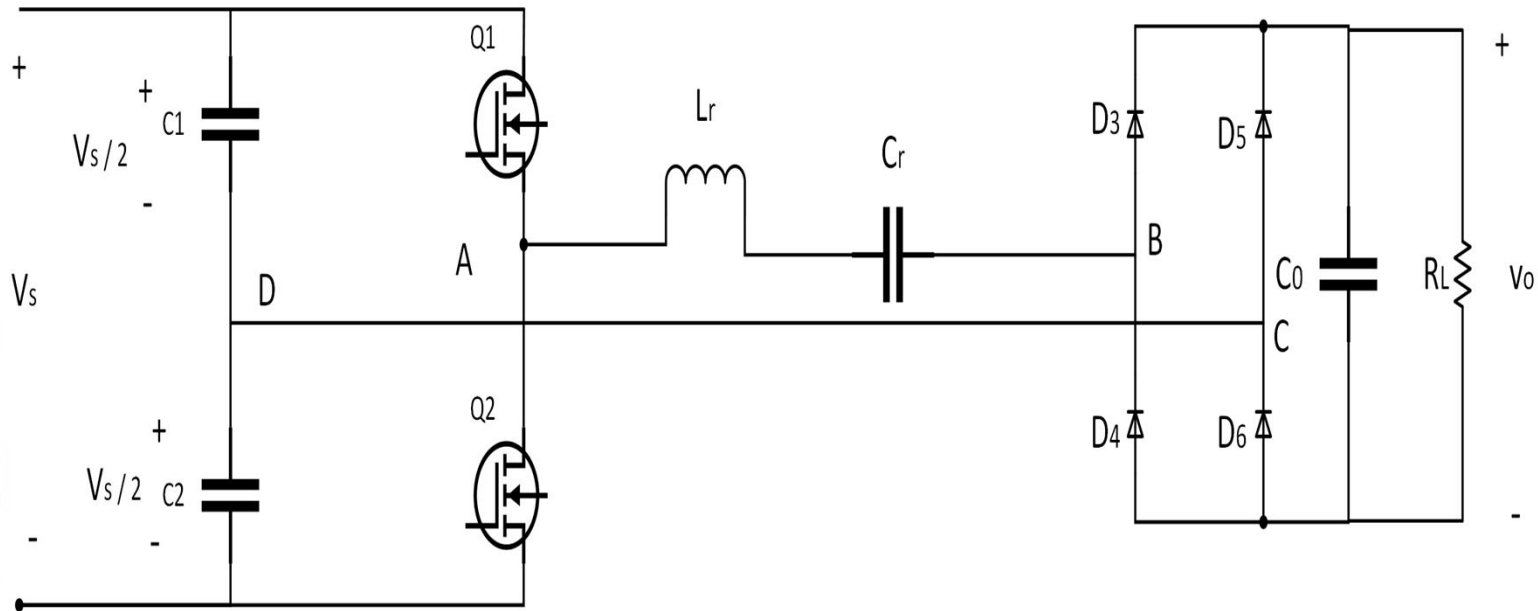
Fig 5: Circuit of a half bridge series resonant converter [2]

Mode1: Discontinuous mode ($0 < f < 0.5f_n$)
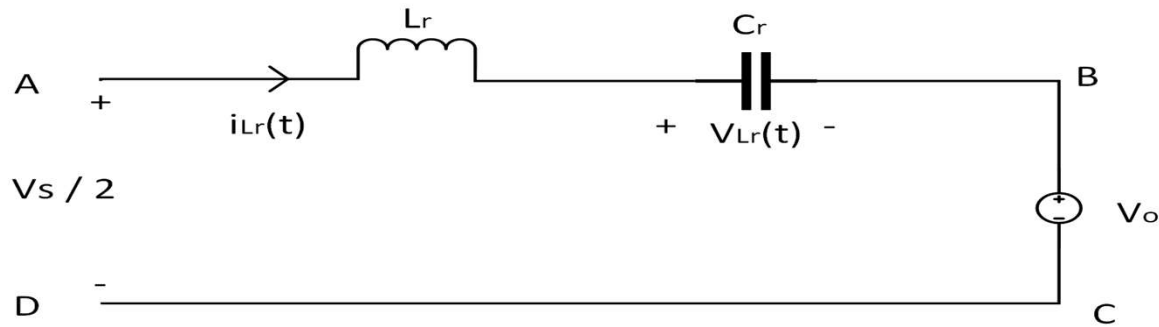
Applying KVL in the circuit ABCD we get,

$$\frac{V_s}{2} - L_r \frac{di}{dt} - \frac{1}{C_r}\int i_{Lr}\,dt - V_o = 0 \qquad (1)$$

Taking Laplace transform

$$\frac{V_s}{2S} - L_r S\,I(S) - \frac{1}{C_r S}I(S) - \frac{V_o}{S} = 0 \qquad (2)$$

$$\frac{V_s}{2S} = L_r S\,I(S) + \frac{1}{C_r S}I(S) + \frac{V_o}{S}$$

$$\frac{V_s}{2S} - \frac{V_o}{S} = I(S)\left[L_r S + \frac{1}{C_r S}\right]$$

$$\frac{V_s - 2V_o}{2S} = I(S)\left[\frac{L_r S C_r S + 1}{C_r S}\right]$$

$$I(S) = \frac{(V_s - 2V_o)C_r}{2(L_r S^2 C_r + 1)} \tag{3}$$

Dividing by Lr and multipling by $\frac{1}{\sqrt{L_r C_r}}$

$$I(S) = \frac{\left(\frac{V_s - 2V_o}{L_r}\right) * \frac{1}{\sqrt{L_r C_r}}}{\left(S^2 + \frac{1}{L_r C_r}\right) * \frac{1}{\sqrt{L_r C_r}}} \tag{4}$$

w.k.t $\dfrac{a}{s^2 + a^2} = \sin a t$

$$I(S) = \left(\dfrac{V_s - 2V_o}{L_r} \right) \sin\left(\dfrac{1}{\sqrt{L_r C_r}} * t \right) * \sqrt{L_r C_r}$$

$$I(S) = \left(\dfrac{V_s - 2V_o}{\sqrt{\dfrac{L_r}{C_r}}} \right) \sin\left(\dfrac{1}{\sqrt{L_r C_r}} * t \right)$$

$$\boxed{i_{Lr}(t) = \left(\dfrac{V_s - 2V_o}{Z_o} \right) \sin\left(\omega_n t \right)} \qquad\qquad \textbf{(5)}$$

$$\omega_n = \dfrac{1}{\sqrt{L_r C_r}} \qquad\qquad Z_o = \sqrt{\dfrac{L_r}{C_r}}$$

18

Solving for $V_{cr}(t)$

$$\frac{dV_{cr}(t)}{dt} = \frac{\dfrac{V_s - 2V_o}{\sqrt{\dfrac{L_r}{C_r}}}\sin(\omega_n t)}{C_r} \tag{6}$$

Integrating the above equation we get

$$V_{cr}(t) = \int \frac{\dfrac{V_s - 2V_o}{\sqrt{\dfrac{L_r}{C_r}}}\sin(\omega_n t)}{C_r}\, dt$$

$$V_{cr}(t) = \frac{V_s - 2V_o}{\sqrt{L_r C_r}}\sqrt{L_r C_r}\int \sin(u)\, du \qquad u = \frac{t}{\sqrt{L_r C_r}}$$

$$V_{cr}(t) = \frac{V_s - 2V_o}{\sqrt{L_r C_r}} \sqrt{L_r C_r} \left(-\cos\left(\frac{t}{\sqrt{L_r C_r}} \right) \right)$$

$$V_{cr}(t) = \frac{V_s - 2V_o}{2} - \cos\left(\frac{t}{\sqrt{L_r C_r}} \right) \left(V_s - 2V_o \right)$$

$$V_{cr}(t) = \frac{V_s}{2} - V_o - \left(V_s - 2V_o \right) \cos\left(\omega_n t \right) \tag{7}$$

$$\omega_n = \frac{1}{\sqrt{L_r C_r}} \qquad Z_o = \sqrt{\frac{L_r}{C_r}}$$
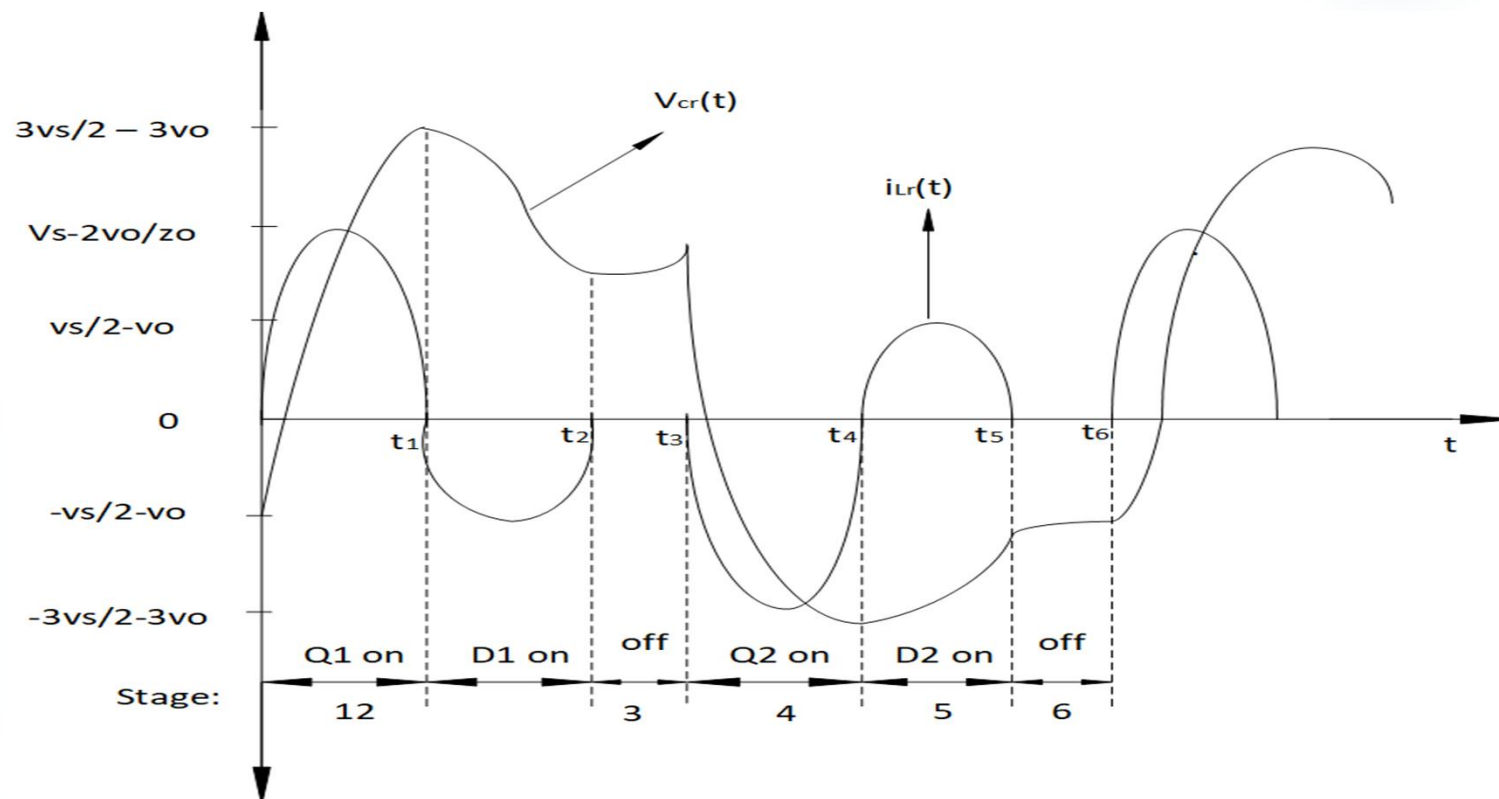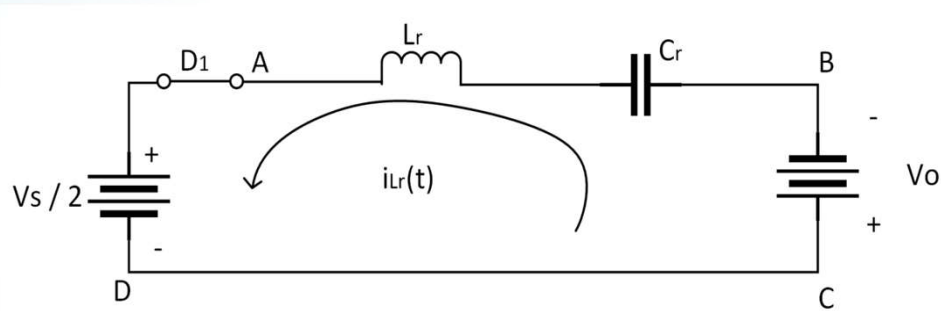
Fig 6: waveform of discontinuous mode of series resonant converter [2]

Mode 2: Continuous Mode (fs > fn or above resonant mode)
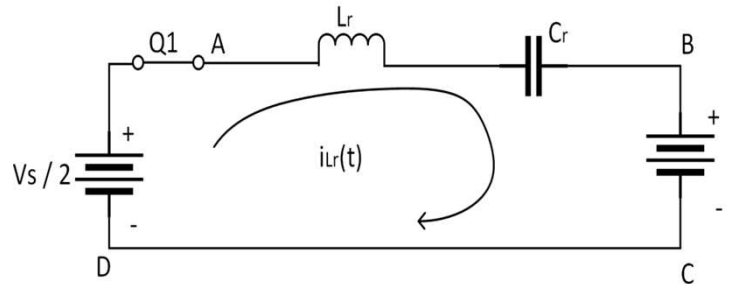
7(a) Stage 1 (0 < t ≤ t1)
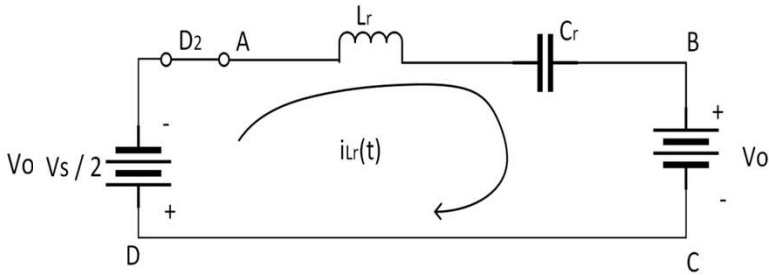
7(b) Stage 2 (t1< t ≤ t2)

7(c) Stage 3 (t2 < t ≤ t3)

Applying KVL in the circuit

$$V_s = L_r \frac{di}{dt} + \frac{1}{C_r} \int i_{Lr} dt + V_o \qquad (8)$$

Taking laplace transform we get

$$\frac{V_s}{2S} = L_r S I(S) - I(O^-) + \frac{I(S)}{C_r S} + \frac{V_o}{S} + V_c(O^-) \qquad (9)$$

$$\frac{V_s}{2S} - \frac{V_o}{S} = I(S) \left[L_r S + \frac{1}{C_r S} \right] - I(O^-) + V_c(O^-)$$

$$I(S) = \frac{\left(\dfrac{V_s}{2S} - \dfrac{V_o}{S} \right) + I(O^-) - V_c(O^-)}{\left[L_r S + \dfrac{1}{C_r S} \right]}$$

30-03-2023

$$I(S) = \frac{\left(\dfrac{V_s - 2V_o}{2S}\right)}{\left[L_r S + \dfrac{1}{C_r S}\right]} + \frac{+I(O^-)}{\left[L_r S + \dfrac{1}{C_r S}\right]} - \frac{V_c(O^-)}{\left[L_r S + \dfrac{1}{C_r S}\right]}$$

$$I(S) = \frac{(V_s - 2V_o)\dfrac{1}{\sqrt{L_r C_r}}}{\dfrac{2L}{\sqrt{L_r C_r}}\left[(S^2) + \left(\dfrac{1}{\sqrt{LC}}\right)^2\right]} + \frac{+I(O^-)S\dfrac{1}{\sqrt{L_r C_r}}}{\dfrac{L}{\sqrt{L_r C_r}}\left[(S^2) + \left(\dfrac{1}{\sqrt{LC}}\right)^2\right]} - \frac{V_c(O^-)S\dfrac{1}{\sqrt{L_r C_r}}}{\dfrac{L}{\sqrt{L_r C_r}}\left[(S^2) + \left(\dfrac{1}{\sqrt{LC}}\right)^2\right]}$$

$$I(S) = \sqrt{\frac{C_r}{L_r}}\frac{(V_s - 2V_o)}{2}\sin\frac{t}{\sqrt{L_r C_r}} + \sqrt{\frac{C_r}{L_r}}\left(I(O^-)\left(\cos\left(\frac{t}{\sqrt{L_r C_r}}\right)\frac{1}{\sqrt{L_r C_r}}\right)\right) - \sqrt{\frac{C_r}{L_r}}\left(V_c(O^-)\left(\cos\left(\frac{t}{\sqrt{L_r C_r}}\right)\frac{1}{\sqrt{L_r C_r}}\right)\right)$$

$$i_{Lr}(t)= \frac{((V_S -2V_o -V_{Cr}(0)))}{Z_n}\sin(\omega_n t)+i_{Lr}(0)\cos(\omega_n t)$$

$$i_{Lr}(t)= \frac{-((V_S -2V_o -V_{Cr}(t_1)))}{Z_n}\sin(\omega_n t)+i_{Lr}(t_1)\cos(\omega_n t) \qquad (10)$$

Solving for $V_{cr}(t)$

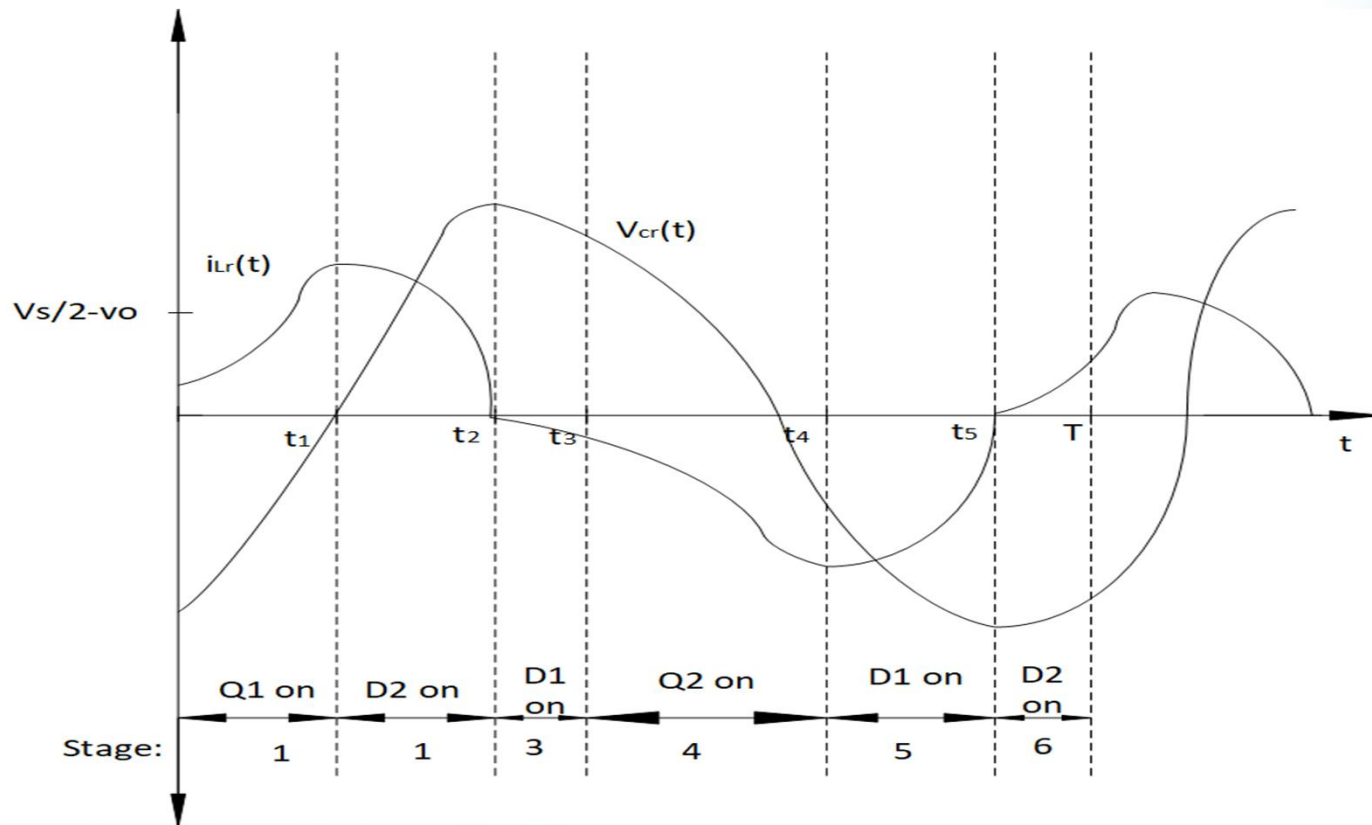$$\frac{dV_{cr}(t)}{dt} = \frac{i_{Lr}(t)}{C_r} \qquad (11)$$

$$\frac{dV_{cr}(t)}{dt} = \frac{\sqrt{\frac{C_r}{L_r}}\frac{(V_s-2V_o)}{2}\sin\frac{t}{\sqrt{L_rC_r}}+\sqrt{\frac{C_r}{L_r}}\left(I(O^-)\left(\cos\left(\frac{t}{\sqrt{L_rC_r}}\right)\frac{1}{\sqrt{L_rC_r}}\right)\right)-\sqrt{\frac{C_r}{L_r}}\left(V_c(O^-)\left(\cos\left(\frac{t}{\sqrt{L_rC_r}}\right)\frac{1}{\sqrt{L_rC_r}}\right)\right)}{C_r}$$
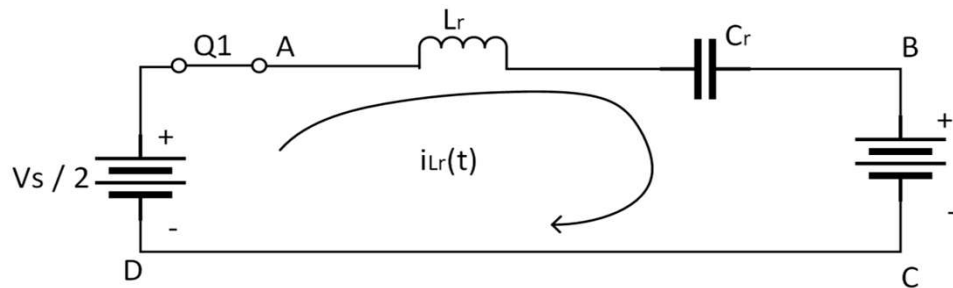
25

Integrating the above equation we get

$$V_{cr}(t)=\int \frac{\sqrt{\frac{C_r}{L_r}}\frac{(V_s-2V_o)}{2}\sin\frac{t}{\sqrt{L_rC_r}}+\sqrt{\frac{C_r}{L_r}}\left(I(O^-)\left(\cos\left(\frac{t}{\sqrt{L_rC_r}}\right)\frac{1}{\sqrt{L_rC_r}}\right)\right)-\sqrt{\frac{C_r}{L_r}}\left(V_c(O^-)\left(\cos\left(\frac{t}{\sqrt{L_rC_r}}\right)\frac{1}{\sqrt{L_rC_r}}\right)\right)}{C_r}dt$$

$$V_{Cr}(t)=\left(\frac{V_s}{2}-V_o\right)-\left(\frac{Vs}{2}-V_o-V_{Cr}(0)\cos(\omega_n t)\right)+i_{Lr}(0)Z_o\sin(\omega_n t)$$

$$\boxed{V_{Cr}(t)=-\left(\frac{V_s}{2}+V_o\right)+\left(\frac{Vs}{2}+V_o+V_{Cr}(t_2)\cos(\omega_n t)\right)+i_{Lr}(t_1)Z_o\sin(\omega_n t)} \qquad \textbf{(12)}$$
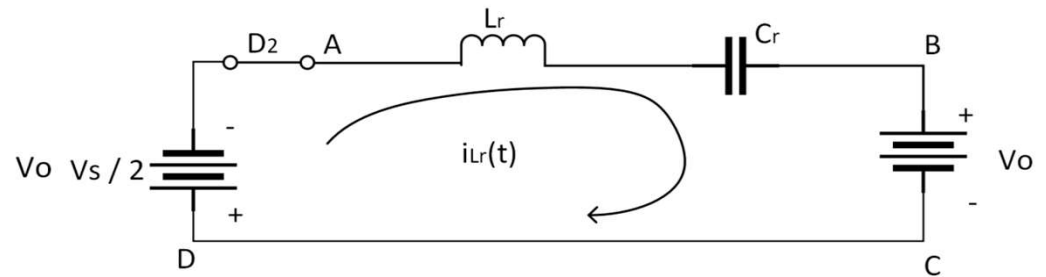
30-03-2023

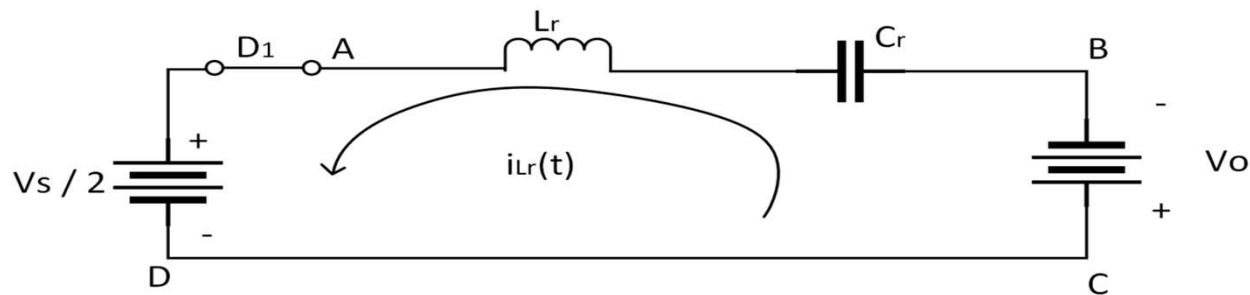**Fig 8: waveform of continuous mode for above resonance of series resonant converter [2]**

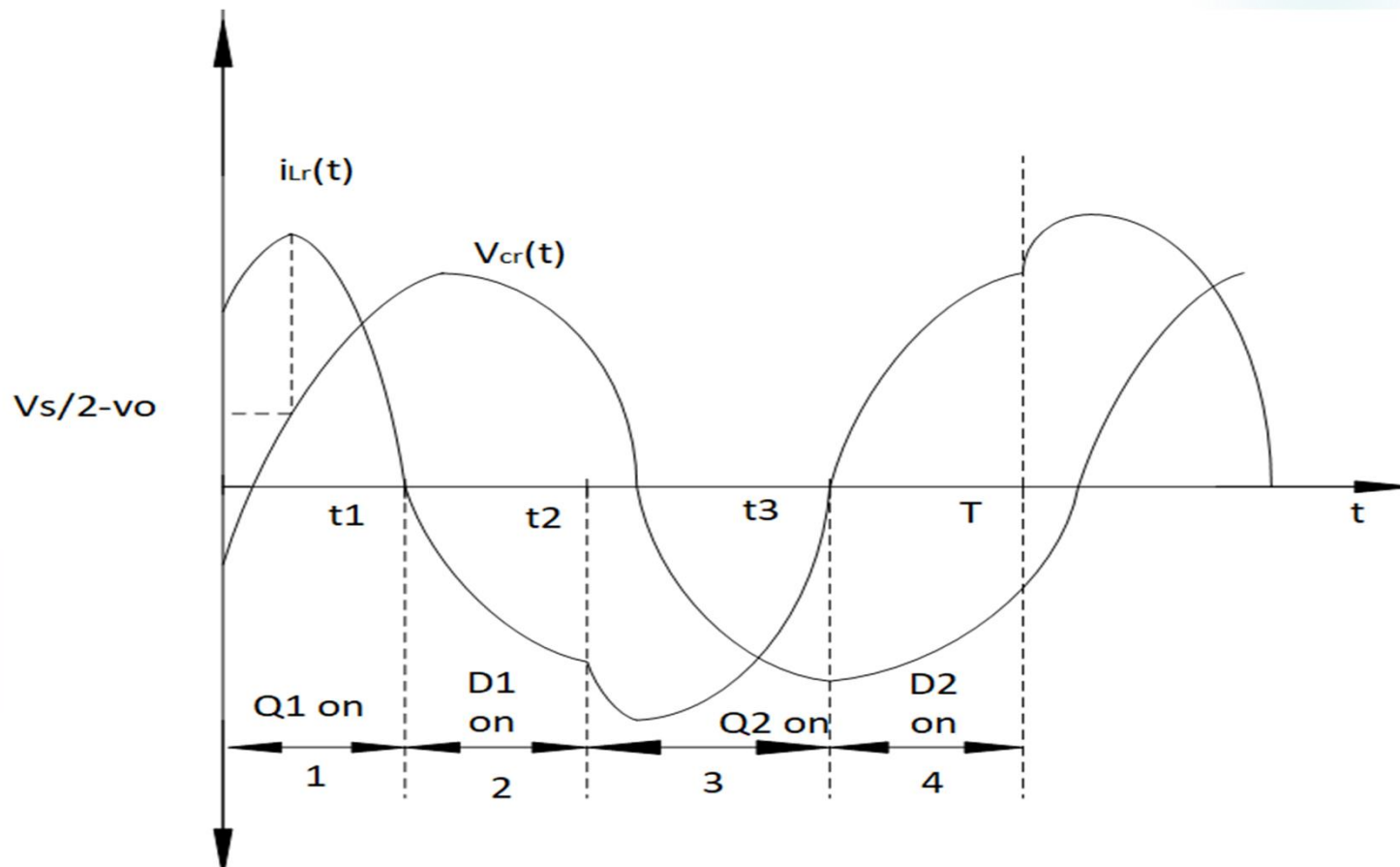# Mode 3: Continuous Mode (fs > fn or above resonant mode)

9(a) Stage 1 (0 < t ≤ t1)

9(b) Stage 2 (t1< t ≤ t2)

9(c) Stage 3 (t2 < t ≤ t3)

Fig 10: waveform of continuous mode for below resonance of series resonant converter [2]

Table 6: Different parameters with values

Parameters	values
Input Voltage (V_{in})	40V
Resonant Frequency (f_o)	200Khz
Impedance (R_o)	6.15Ω
Output Current (I_o)	12A
Output Voltage (V_o)	12V
Output Power (P_o)	144W

30-03-2023

7. Modeling

1) Modeling of series resonant converter with First Harmonic Approximation (FHA)

On the input side, the fundamental voltage of the square-wave voltage (Vsq) is

$$V_{ge}(t) = \frac{2}{\pi} * V_{DC} * \sin(2\pi f_{sw}t) \tag{14}$$

RMS value is

$$V_{ge} = \frac{\sqrt{2}}{\pi} * V_{DC} \tag{15}$$

On the output side, since Vso is approximated as a square wave, the fundamental voltage is

$$V_{oe}(t) = \frac{4}{\pi} * n * V_o * \sin(2\pi f_{sw}t - \phi_V) \tag{16}$$

the phase angle between Voe and Vge, and the RMS output voltage is

$$V_{oe} = \frac{2\sqrt{2}}{\pi} * n * V_o \tag{17}$$

30-03-2023

The fundamental component of current corresponding to Voe and Ioe is

$$i_{oe}(t) = \frac{\pi}{2} * \frac{1}{n} * I_o * \sin(2\pi f_{sw}t - \phi_i)$$
(18)

and the RMS output current is

$$I_{oe} = \frac{\pi}{2\sqrt{2}} * \frac{1}{n} * I_o$$
(19)

Then the AC equivalent load resistance, Re, can be calculated as

$$R_e = \frac{V_{oe}}{I_{oe}} = \frac{8*n^2}{\pi^2} * \frac{V_o}{I_o} = \frac{8*n^2}{\pi^2} * R_L$$
(20)

$$\omega_{sw} = 2\pi f_{sw}$$
(21)

which can be simplified as

$$\omega = \omega_{sw} = 2\pi f_{sw} \qquad (22)$$

The capacitive and inductive reactance of Cr and Lr respectively, are

$$X_{C_r} = \frac{1}{\omega C_r} \qquad\qquad X_{L_r} = \omega L_r$$

the relationship between the input voltage and output voltage can be described by their ratio or gain

$$M_{g\_min} = \frac{n*(V_{o\_min} + V_F)}{V_{in\_min}/2} \qquad (23)$$

the DC input voltage and output voltage are converted into switching mode

$$M_{g\_max} = \frac{n*(V_{o\_max} + V_F + V_{loss})}{V_{in\_min}/2} \qquad (24)$$

30-03-2023

Determine the Equivalent Load Resistance (Re)

$$R_e = \frac{8 * n^2}{\pi^2} * \frac{V_o}{I_o}$$ (25)

Voltage-Gain Function

the relationship between the input voltage and output voltage can be described by their ratio or gain:

$$M_{g\_DC} = \frac{n \times V_o}{\frac{V_{in}}{2}} = \frac{n \times V_o}{\frac{V_{DC}}{2}}$$ (26)

$$M_{g\_DC} \approx M_{g\_sw} = \frac{V_{so}}{V_{sq}}$$

input-to-output voltage-gain or voltage-transfer function becomes

$$M_g = \frac{V_{oe}}{V_{ge}} = \left| \frac{jX_{Lm} P R_e}{(jX_{Lm} P R_e) + j(X_{Lr} - X_{Cr})} \right|$$ (27)

34

$$V_o = M_g \times \frac{1}{n} \times \frac{V_{in}}{2} \qquad (28)$$

the normalized frequency is expressed as

$$f_n = \frac{f_{sw}}{f_o} \qquad (29)$$

The quality factor of the series resonant circuit is defined as

$$Q_e = \frac{\sqrt{\dfrac{L_r}{C_r}}}{R_e} \qquad (30)$$

the voltage gain function can then be normalized and expressed as

$$M_g = \left| \frac{L_n \times f_n^2}{[(L_n + 1) \times f_n^2 - 1] + j[(f_n^2 - 1) \times f_n \times Q_e \times L_n]} \right| \qquad (31)$$

The relationship between input and output voltages can also be obtained from

$$V_o = M_g \times \frac{1}{n} \times \frac{V_{in}}{2} = M_g(f_n, L_n, Q_e) \times \frac{1}{n} \times \frac{V_{DC}}{2} \qquad (32)$$

where $V_{in} = V_{DC}$
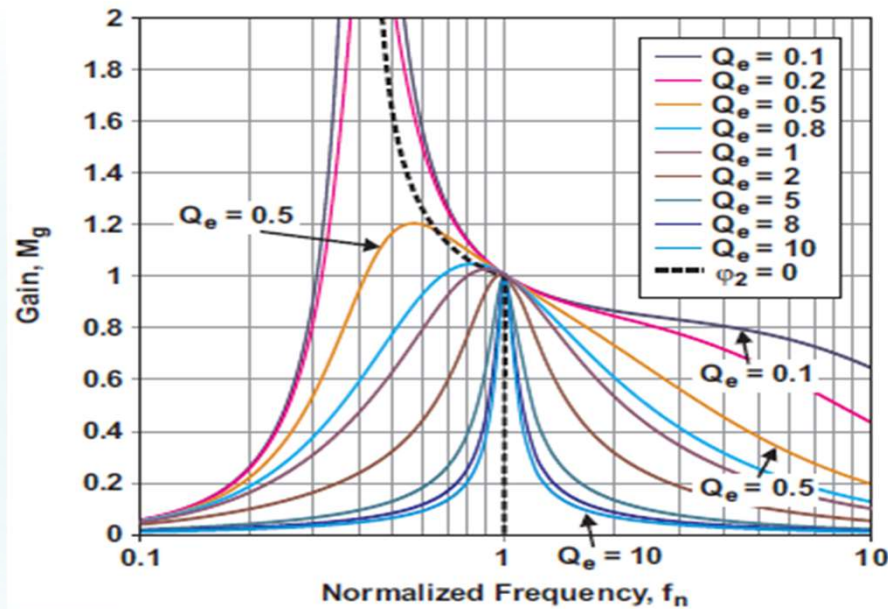
Fig 11: Plots of voltage-gain function [4]

2) Modeling of series resonant converter with Small Signal

Small Signal Steady State Relations for Resonant Converters

- **Finding an operating point for a stable state is the first step in the dynamic analysis of resonant converters. In particular, the steady state behavior of parallel and series resonant converters is covered in this section.**

- **For such a normalised switching frequency F = Fs/Fo given by the series resonant converter, the kth continuous conduction mode arises.**

$$\frac{1}{(k+1)} < F < \frac{1}{k} \tag{33}$$

30-03-2023

- the normalised dc output voltage is represented by

$$M = \frac{V}{V_g} \qquad (34)$$

- Currents are represented by the letter J and normalised with respect to the base current Vg/Ro, where Ro is the tank's characteristic impedance.

$$J = \frac{1}{\left(V_g / R_o\right)} \qquad (35)$$

- These inductor current & tank capacitor voltage changes can be expressed in writing as follows:

$$\frac{\Delta V_c(t)}{\frac{T_s}{2}} = \frac{-V_c\left(\frac{t_s}{2}\right) - V_c(0)}{\frac{T_s}{2}} \qquad \frac{\Delta i_L(t)}{\frac{T_s}{2}} = \frac{-i_L\left(\frac{t_s}{2}\right) - i_L(0)}{\frac{T_s}{2}} \qquad (36)$$
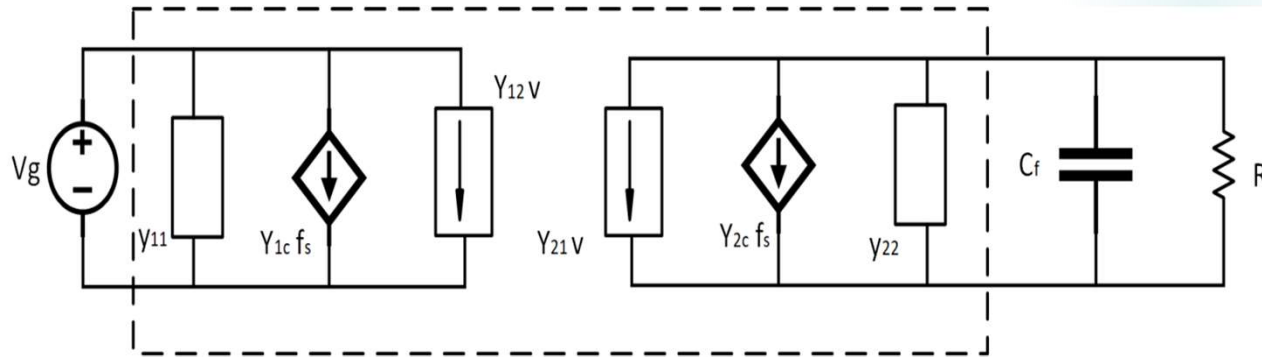
Fig 12: equivalent circuit for the series resistor converter's y-parameter model using lumped parameters

the control to output transfer function is

$$\frac{\hat{v}}{f_s}(s) = -K_{2c}R \,||\, R_{22} \frac{1}{1 + sC_F R \,||\, R_{22}}$$

(37)

the slope of the control curve is given as

$$\frac{\partial v}{\partial f_s} = -K_{2c}R \,||\, R_{22}$$

(38)

the control transfer function's dc gain is

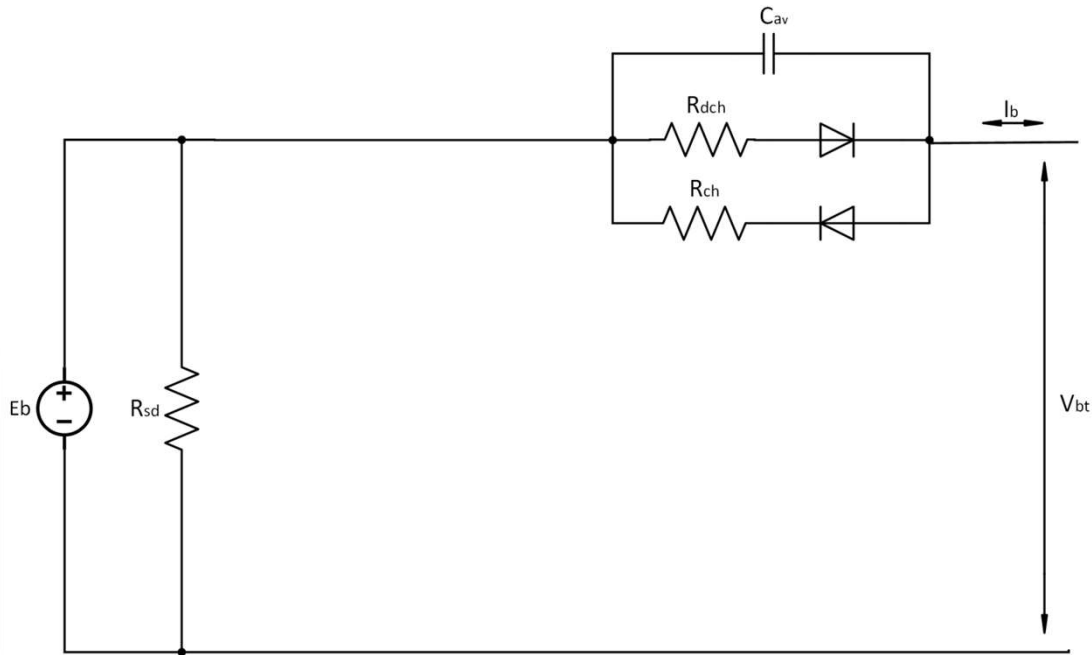$$\frac{\hat{v}}{\hat{f}_s}(0) = K_{2c}\frac{R}{R + R_{22}}$$

(39)

Modeling of lead acid battery

Fig 13: Dynamic Model of a Lead-Acid Battery [7]

The terminal voltages of the battery are derived as:

$$V_{bt\_charging} = E_b + I_b R_{ch}\left(1 - e^{\frac{-t}{R_{ch}C_{av}}}\right) \tag{40}$$

$$V_{bt\_discharging} = E_b - I_b R_{dch} \left(1 - e^{\frac{-t}{Rd_{ch}C_{av}}} \right) \tag{41}$$

Using the linear approximation technique, a function between Eb and SOC is given by:

$$E_b = 0.01375 SOC + 11.5 \tag{42}$$

$$R_{sd} = -0.039 SOC^2 + 4.27 SOC - 19.23 \tag{43}$$

the resistance Rdch is divided into two components

$$R_{dch} = R_{dbi} + R_{db} \tag{44}$$

where

$$R_{bdi} = 1.01 e^{-2.21 I_b} + 0.24 e^{-0.06 I_b} \tag{45}$$

30-03-2023

$$R_{bd} = 2.926e^{-0.042SOC}$$

(46)

During charging, Rch can be divided into two components

$$R_{ch} = R_{bci} + R_{bc}$$

(47)

$$R_{bc} = 9.32 * 10^{-5}SOC^2 + 0.01SOC + 0.028$$

(48)
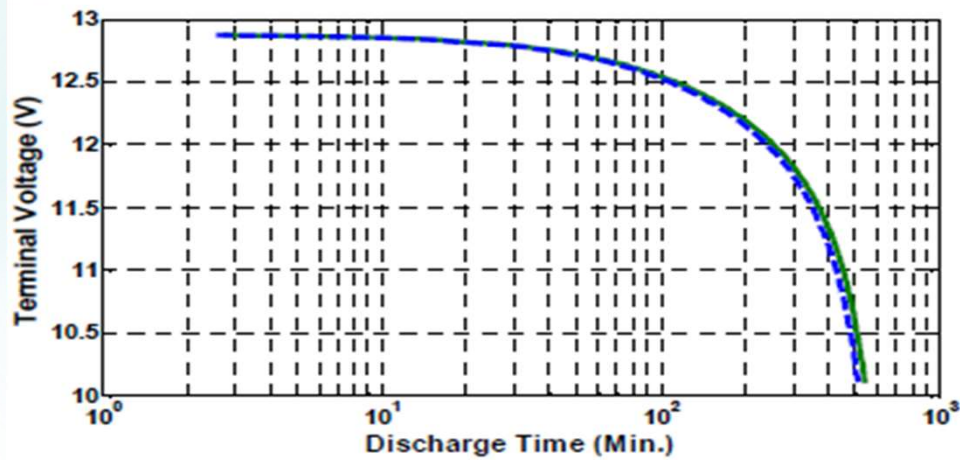
Fig. 14- Validation Results of the Battery Model at 0.1 CA [10]

Modeling of Photovoltaic systems

Generally, the I-V characteristic for a PV module composed of series connected cells is expressed as follows

$$I = I_{ph} - I_s \left[e^{\left(\frac{q(V + IR_s N_s)}{N_s KTA} \right)} - 1 \right] - \frac{(V + IR_s N_s)}{(N_s R_{sh})} \tag{48}$$

$$I = I_{ph} - I_s \left[e^{\left(\frac{qV}{N_s KAT} \right)} - 1 \right]$$

Iph is determined from manufacturer datasheets, as follows:

$$I_{ph} = G \left(I_{sc} + \alpha \Delta T \right) \tag{49}$$

$$V_{oc}(G,T) - V_{oc}(G,T_o) = -\left| \beta \right| \Delta T \tag{50}$$

the open circuit voltage formula is determined as

$$V_{oc} = \frac{N_s K T A}{q} \ln \left(\frac{I_{ph}}{I_s} + 1 \right) \tag{51}$$

$$I_s = \frac{e^{\frac{|\beta| \Delta T q}{N_s K T A}} G \left[I_{sc} + \alpha \Delta T \right]}{\left(G I_{sc} / I_{rs} + 1 \right)^{\frac{T_o}{Y}} - e^{\frac{|\beta| \Delta T q}{N_s K T A}}} \tag{52}$$

$$I_{rs} = \frac{I_{sc}}{\left[e^{\left(\frac{q V_{oc}}{N_s K A T_o} \right)} - 1 \right]} \tag{53}$$

$$I_m = I_{sc} - I_{rs} \left[e^{\left(\frac{q V_m}{N_s K A T_o} \right)} - 1 \right] \tag{54}$$

$$\frac{I_m}{I_{sc}} = e^{\frac{q V_m}{N_s K T_o A}} - \left(\frac{I_{sc} - I_m}{I_{sc}} \right) e^{\frac{q V_{oc}}{N_s K T_o A}} \tag{55}$$

44

8. DESIGN OF SERIES RESONANT CONVERTER

Photovoltaic panel (supply)

Output voltage :   35V to 40V

Output current :   4A to 6A

Power   :   190W to 210W

UPS Battery (Load)

Input Voltage :   11V to 13V

Input Current :   12V to 14V

Power   :   140W to 160W

Design Calculation of 150W Series resonant converter

$$n = \frac{V_{in}}{2V_o} = \frac{35}{2(12)} = 1.45 \approx 2$$

$$M_{g\_min} = \frac{n \times \left(V_{o\_min} + V_f\right)}{\dfrac{V_{in\_max}}{2}} = \frac{2 \cdot (12 \cdot (1 - 1\%) + 0.7}{\dfrac{40}{2}} = \mathbf{1.27}$$

$$M_{g\_max} = \frac{n \times \left(V_{o\_max} + V_f + V_{Loss}\right)}{\dfrac{V_{in\_min}}{2}} = \frac{2 \times (15 \times (1 + 1\%) + 0.7 + 1.05}{\dfrac{35}{2}} = \mathbf{1.914}$$

$$R_e = \frac{8 \times n^2}{\pi^2} \times \frac{V_o}{I_o} = \frac{8(2)^2}{\pi^2} \times \frac{12}{12} = 3.2\,\Omega$$

At 110% overload

$$R_e = \frac{8 \times n^2}{\pi^2} \times \frac{V_o}{I_o} = \frac{8(2)^2}{\pi^2} \times \frac{12}{12 \times 110\%} = 2.945\Omega$$

$$C_r = \frac{1}{2\pi \times Q \times f \times R_e} = \frac{1}{2\pi \times 0.5 \times 200 \times 10^3 \times 3.2} = 49.73\text{nF}$$

30-03-2023

$$L_r = \frac{1}{(2\pi f_o)^2 C_r} = \frac{1}{(2\pi \times 200 \times 10^3)^2 \times 49.73 \times 10^{-9}} = 12.733\,\mu H$$

Verify the resonant circuit design

$$f_o = \frac{1}{2\pi \sqrt{L_r C_r}} = \frac{1}{2\pi \sqrt{12.733 \times 10^6 \times 49.73 \times 10^{-9}}} = 200.007\,KHz$$

$$Q = \frac{\sqrt{\dfrac{L_r}{C_r}}}{R_e} = \frac{\sqrt{\dfrac{12.73 \times 10^{-6}}{49.73 \times 10^{-9}}}}{3.2} = 5.004 \approx 5$$

The primary Side Currents

$$I_{oe} = \frac{\pi}{2\sqrt{2}} \times \frac{I_o}{n} = \frac{\pi}{2\sqrt{2}} \times \frac{12 \times 110\%}{2} = 7.326\,A$$

30-03-2023

The secondary side currents

$$I_{oe\_s} = n \times I_{oe} = 2 \times 7.326 = 14.652 \, A$$

$$I_{sw} = \frac{\sqrt{2} \times I_{oe\_s}}{2} = \frac{\sqrt{2} \times 14.652}{2} = 10.36 \, A$$

$$I_r = \sqrt{I_{oe}^2} = 7.326 \, A$$

$$I_{sav} = \frac{\sqrt{2} \times I_{oe\_s}}{\pi} = \frac{\sqrt{2} \times 7.326}{\pi} = 6.595 \, A$$

30-03-2023

9. DESIGN OF CONTROLLER FOR THE SERIES RESONANT CONVERTER

- The control system is a way to maintain any amount in any system, whether it a machine, mechanism, or piece of equipment, as well as to change how it performs.

- The controllers help with automated control of the system's output and increase the converter's steady-state performance and transient responsiveness. Open-loop controls and closed-loop controls are the two different types of controls.

Average Current Mode Control

- An ACMC model is proposed in light of this result and the well-established multi-loop analysis.

- The operating modes, operational area, and four extreme working points of a LC series resonant converter are established for a wide variety of operating situations

30-03-2023
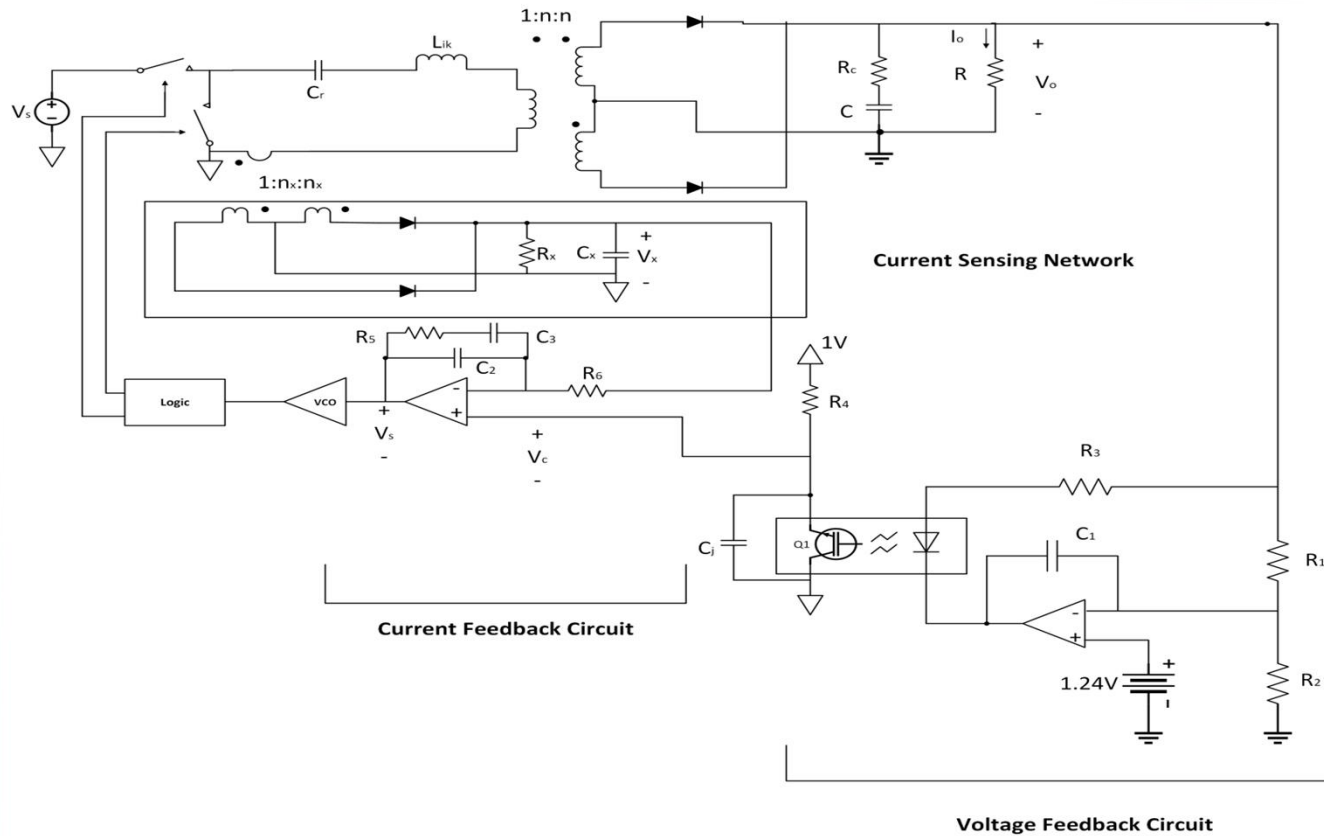
Fig 15: A proposed average current mode control is used in an experimental LC converter.

- The proposed average current-mode control is implemented in the circuit design of the experimental LC converter in Figure 6.1.
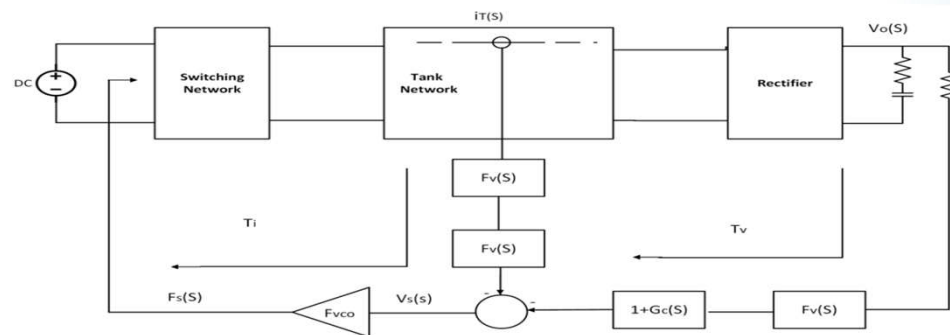
Fig 16: Block diagram of ACMC for Resonant Converters.
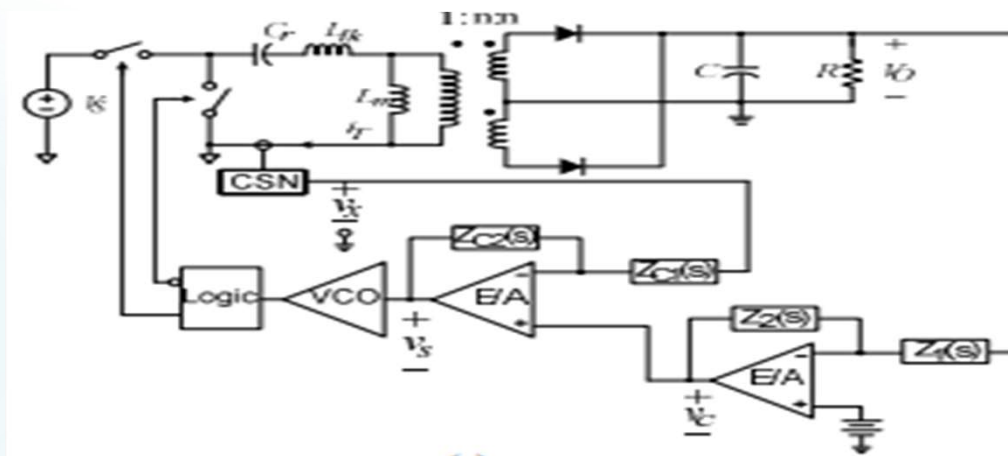
Fig 17: Functional circuit diagram of average current-mode control scheme.

A control-to-output transfer function Gvci(S) is,
$$G_{vci}(s) \equiv \frac{V_o(s)}{V_c(s)}\bigg|_{H_i(s)\neq 0} = \frac{F_{vco}\dfrac{V_o(s)}{f_s(s)}}{1+F_{vco}\dfrac{i_T(s)}{f_s(s)}G_c(s)H_i(s)} \tag{56}$$

Design of a Current Feedback Compensation Gc(S):
$$G_c(s) = \frac{K_C\left(1+s/\omega_{zc}\right)}{s\left(1+\left(s/\omega_{pc}\right)\right)} \tag{57}$$

Design for Voltage Feedback Compensation
$$G_{vci}(s) \cong G_{vci}\frac{\left(1+\dfrac{s}{\omega_{esr}}\right)}{\left(1+\dfrac{s}{\omega_{pl1}}\right)\left(1+\dfrac{s}{Q\omega_o}+\dfrac{s^2}{\omega_o^2}\right)} \tag{58}$$

The output current is taken to be constant for the purposes of deriving the audio-susceptibility transfer function.

$$\frac{\hat{V}_o}{\hat{V}_g} = \frac{G_{vg}\left(1+T_{ii}\right)+F_m\cdot G_{vd}\left[K_f-G_{ig}\left(H_e+G_{ci}\right)R_i\right]}{1+T_{ii}-K_r\cdot F_m\cdot G_{vd}} \tag{59}$$

Output Impedance is given as
$$\frac{\hat{V}_o}{-\hat{I}_o} = \frac{Z_{out}(1+T_{ii}) + G_{vd}F_m G_{iL}(H_e + G_{ci})R_i}{1 + T_{ii} - K_r \cdot F_m \cdot G_{vd}} \qquad (60)$$

Output Voltage to Duty cycle Transfer Function
$$\frac{\hat{V}_o}{\hat{d}} = \frac{\hat{V}_g G_{vg} + \hat{d}G_{vd} - \hat{I}_o Z_{out}}{F_m \left[\hat{V}_g k_f + \hat{V}_o k_r - \hat{I}_L (H_e + G_{ci})R_i\right]} \qquad (61)$$
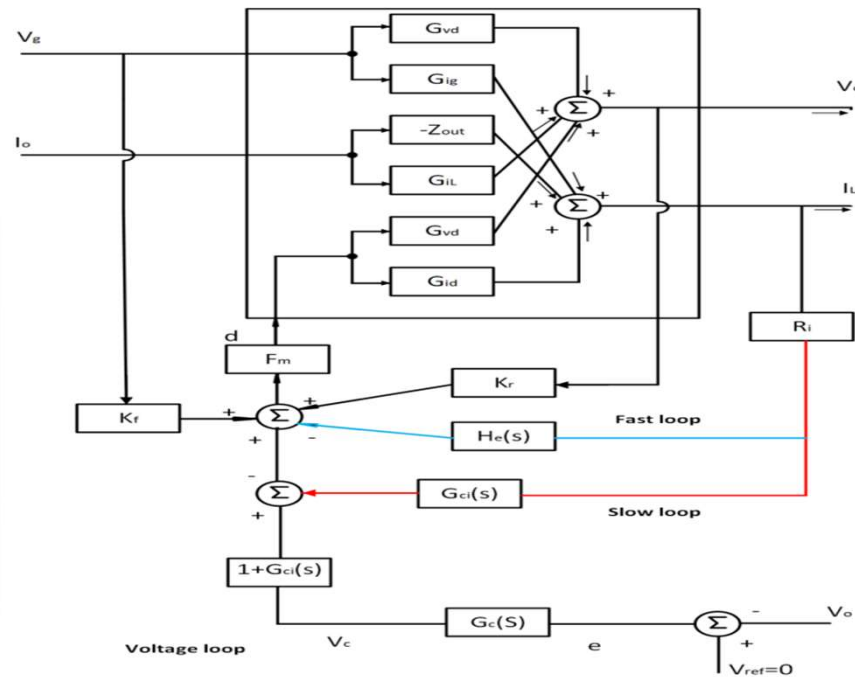

Fig 18: Small-signal ACM control model

53

10. SIMULATION

Matlab Simulation of Photovoltaic module
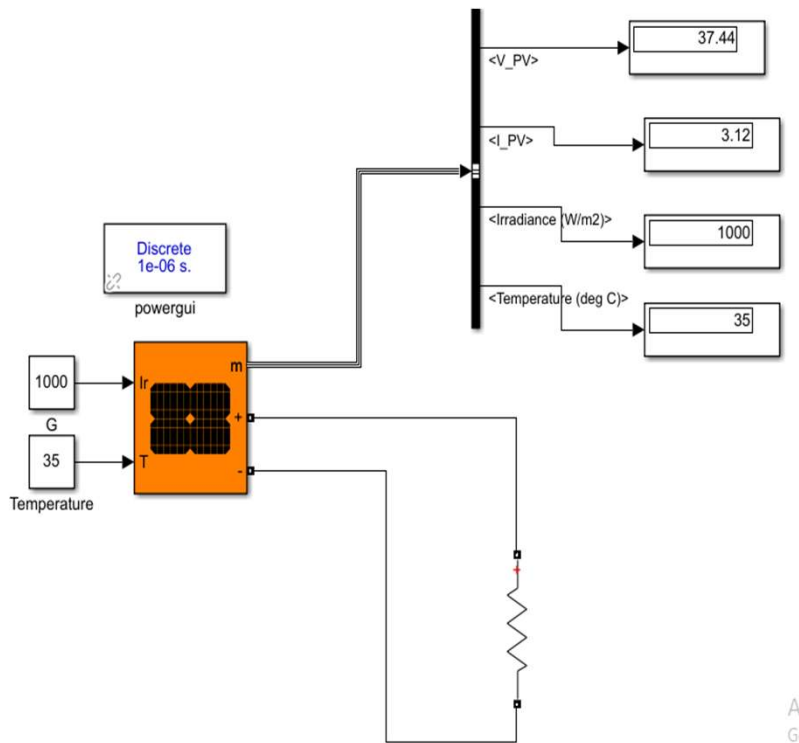
Fig 19: Matlab simulation of Photovoltaic System

Photovoltaic panel (supply)
Output voltage :   35V to 40V
Output current :   3A to 4A
Power   :   190W to 210W

Table 7: Voltage and Current measurements for change in Temperature

Temperature (degrees)	Irradiance (W / m²)	Voltage (V)	Current (I)
25	1000	39.31	3.27
30	1000	38.07	3.17
35	1000	37.44	3.12
40	1000	36.81	3.06
45	1000	36.18	3.01
50	1000	35.55	2.96
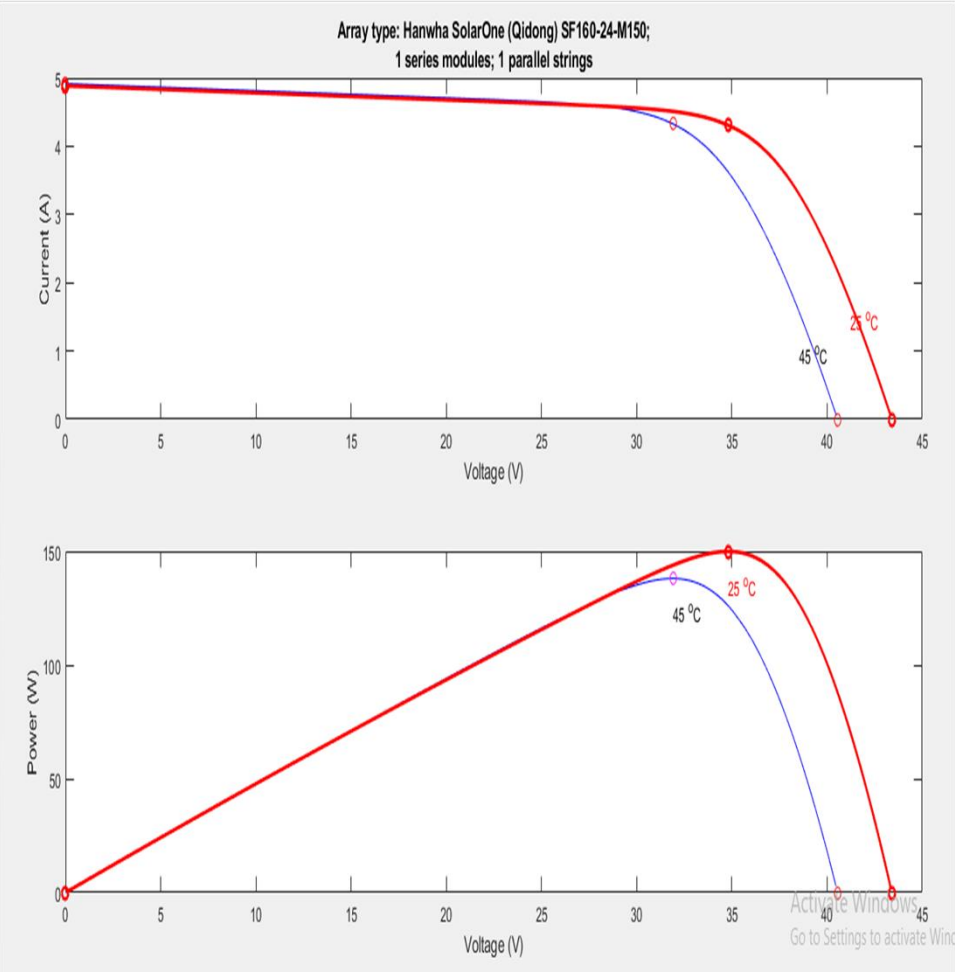
30-03-2023

Fig 20: Plot for voltage, current and power of PV array

30-03-2023

Table 8: Module data

Module	Hanwha SolarOne (Qidong) sf160-24-M150
Maximum Power (W)	149.988W
Cells per module (Ncell)	72
Open circuit voltage Voc (V)	43.4V
Short circuit current Isc (A)	4.88A
Voltage at maximum power point Vmp (V)	34.8V
Current at maximum power point Imp (A)	4.31A
Temperature coefficient of Voc (%/deg.C)	-0.328 %/deg.C
Temperature coefficient of Isc (%/deg.C)	0.033996

Table 9: Model parameters.

Light-generated current IL (A)	4.9254
Diode saturation current I0 (A)	4.7771e-11A
Diode ideality factor	0.92869
Shunt resistance Rsh (ohms)	95.9331
Series resistance Rs (ohms)	0.79087

simulation model of LC resonant converter.
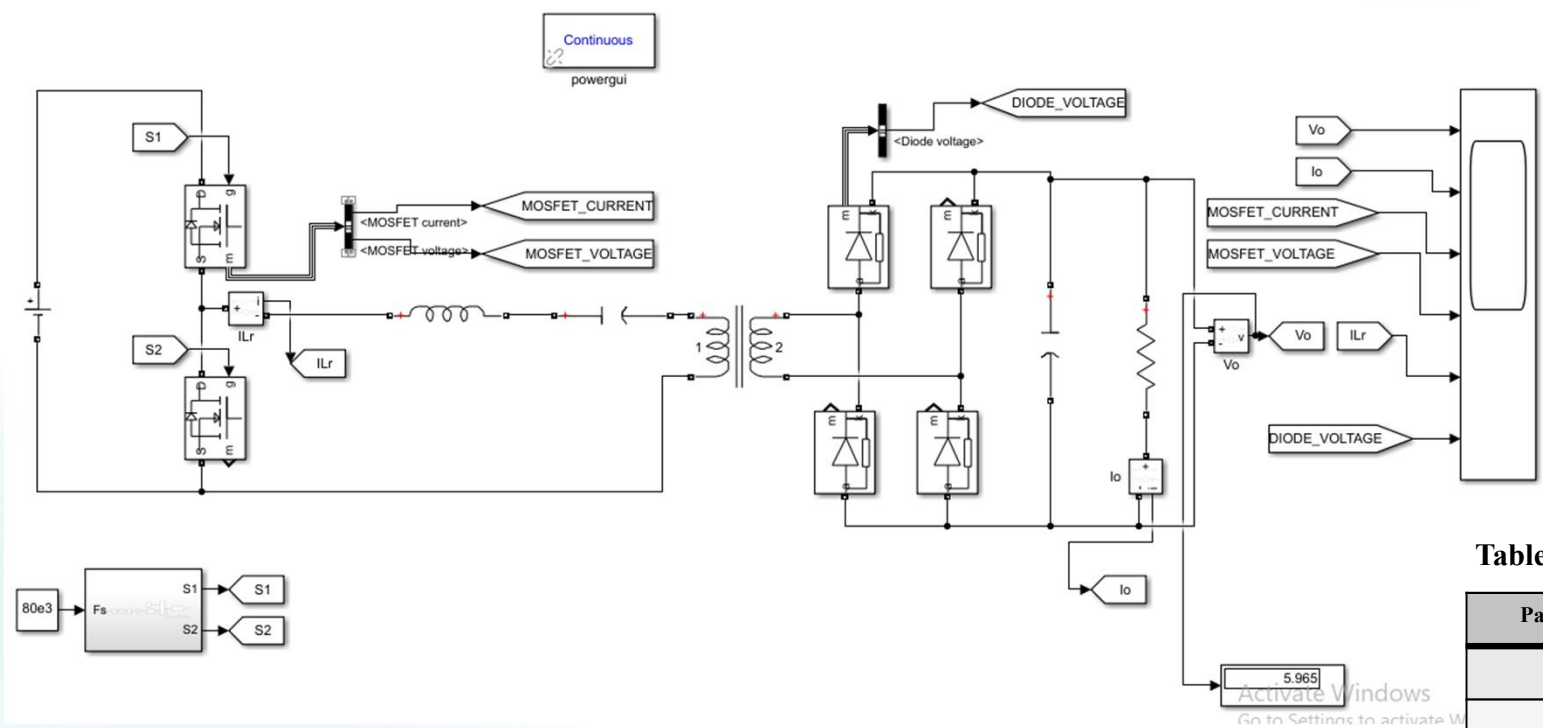
Fig 21: Matlab simulation model of LC resonant converter

Table 10: Different parameters

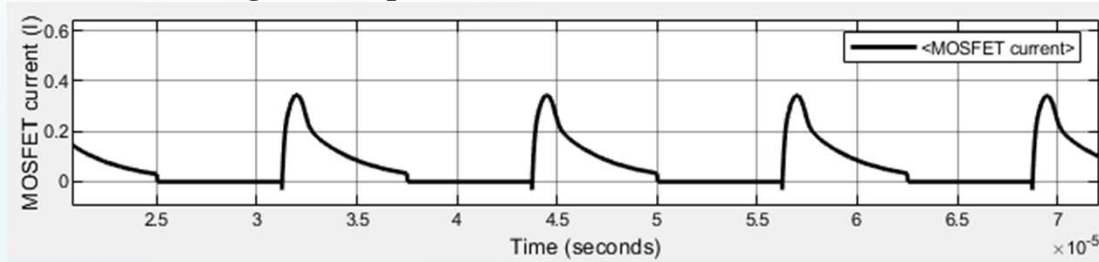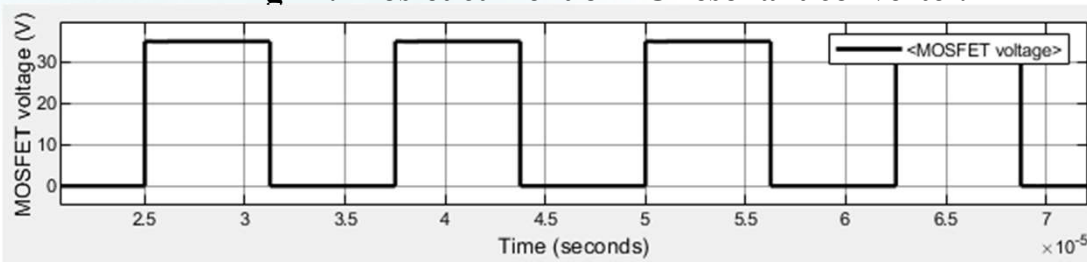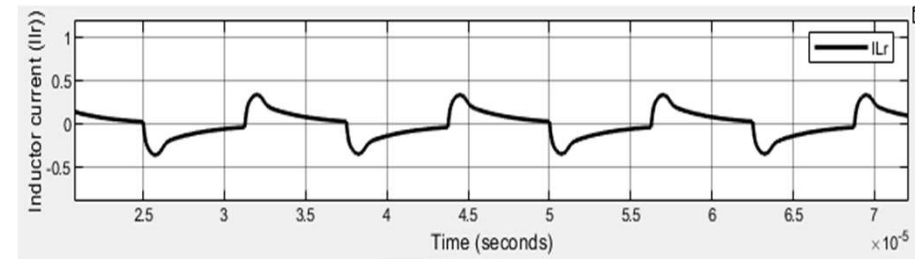| Parameters	values
Vin	40V
f_o	200Khz
Ro	6.15Ω
L	12.733µH
C	49.73µF
Io	0.02A
Vo	6V
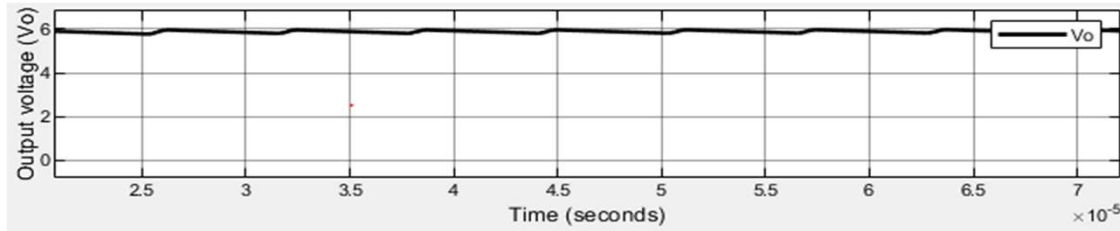
Fig 22: Output voltage of LC resonant converter.
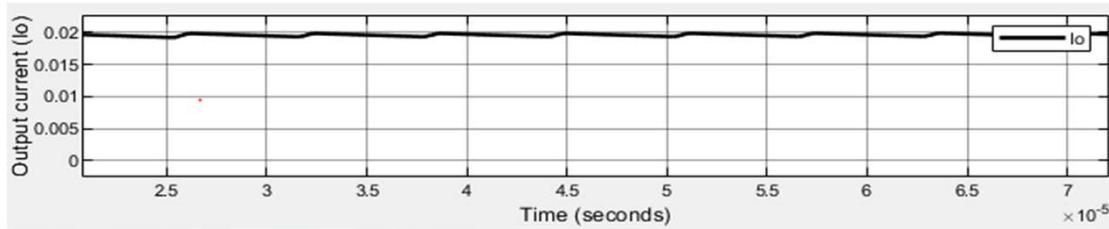
Fig 23: Output current of LC resonant converter.

Fig 24: Mosfet current of LC resonant converter.

Fig 25: Mosfet voltage of LC resonant converter.

Fig 26: Inductor current of LC resonant converter.

57

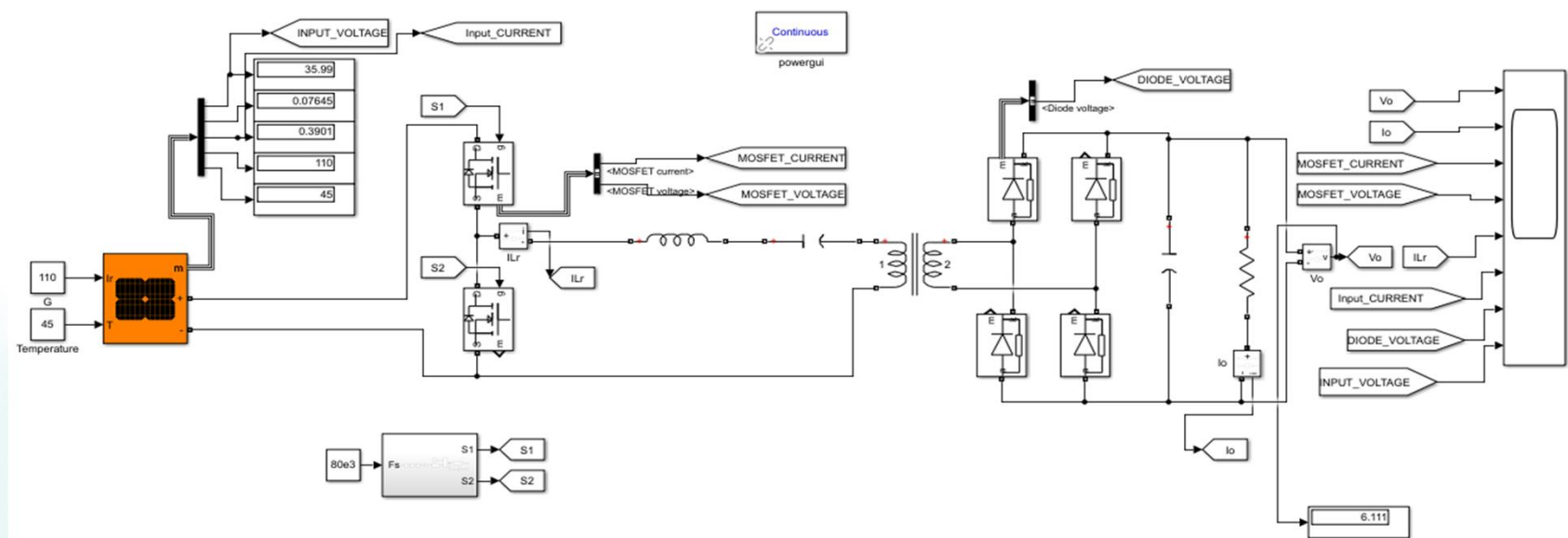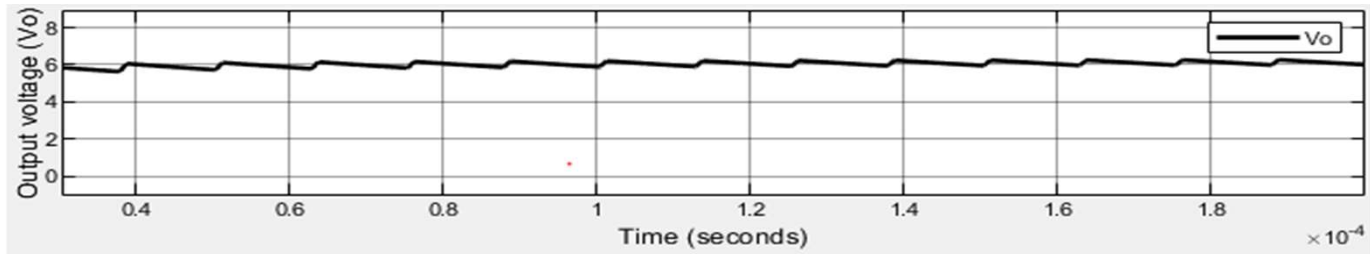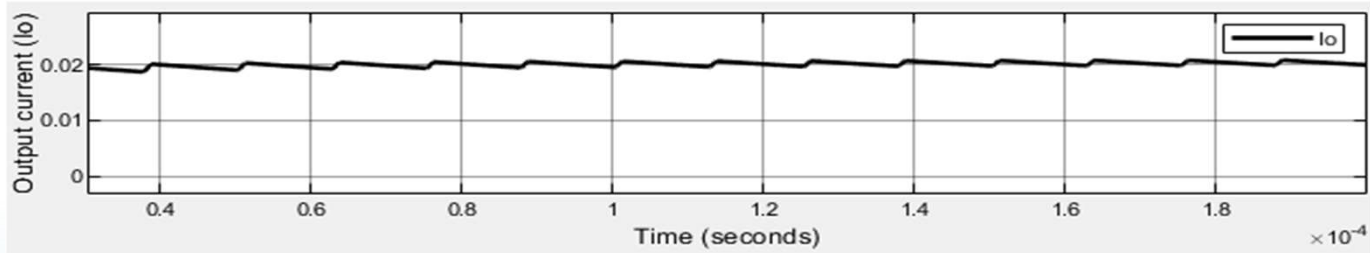# Simulation of PV System with LC Resonant Converter under Open Loop

Fig 27: Matlab simulation for open loop LC resonant converter.
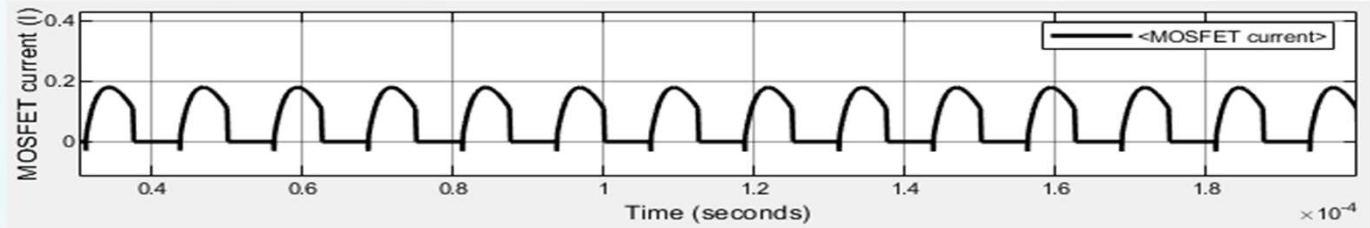
Table 11: Different parameters

Parameters	values
Vin	35V
f_o	200Khz
Ro	6.15Ω
L	12.733µH
C	49.73µF
Io	0.02A
Vo	6.3V

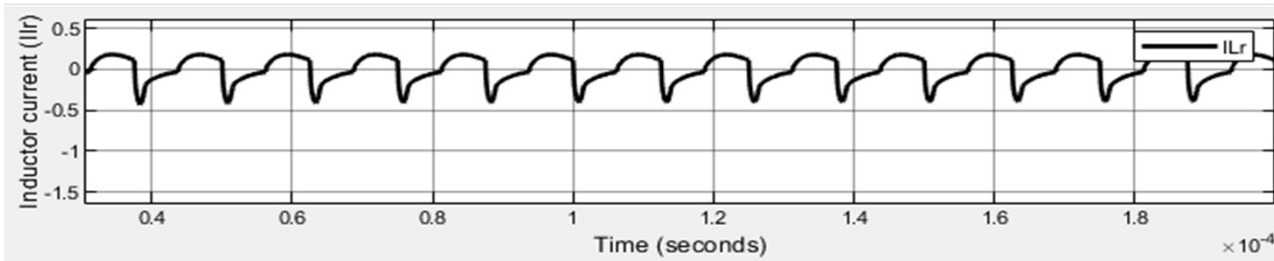**Fig 7.11: Output voltage for open loop LC resonant converter.**

Fig 7.12: Output current for open loop LC resonant converter
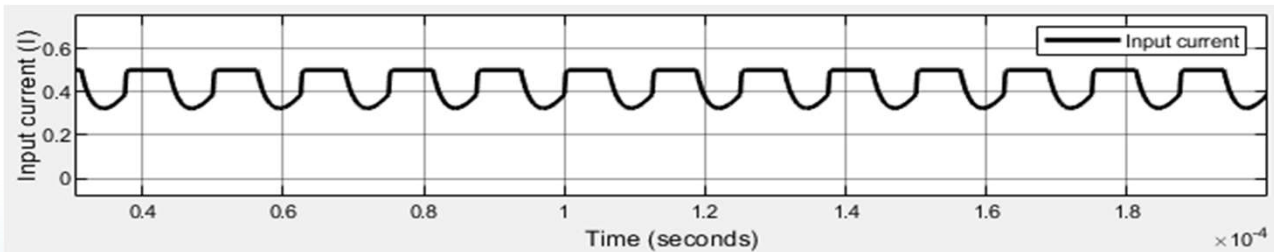

Fig 7.13: Mosfet current for open loop LC resonant converter
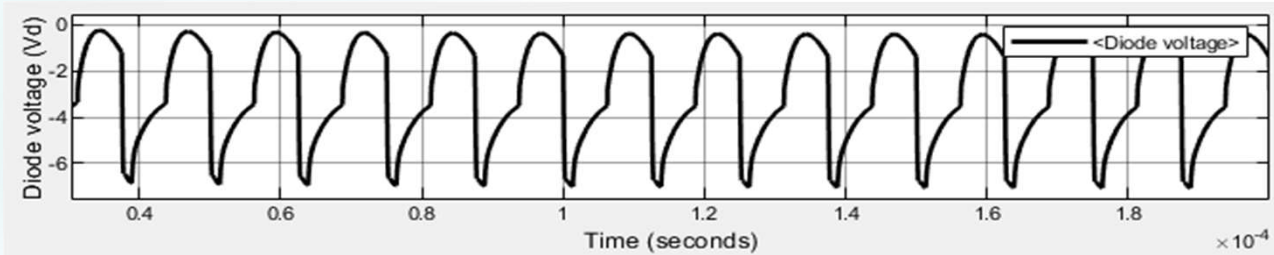

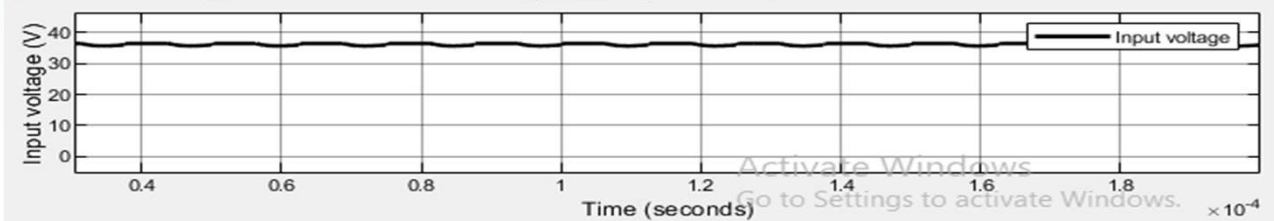**Fig 7.14: Mosfet voltage for open loop LC resonant converter.**

Fig 7.15: Inductor current for open loop LC resonant converter.

Fig 7.16: Input current for open loop LC resonant converter.

Fig 7.17: Diode voltage for open loop LC resonant converter.

Fig 7.18: Input voltage for open loop LC resonant converter.

Simulation of PV System with LC Resonant Converter for UPS Battery Charging under Open Loop
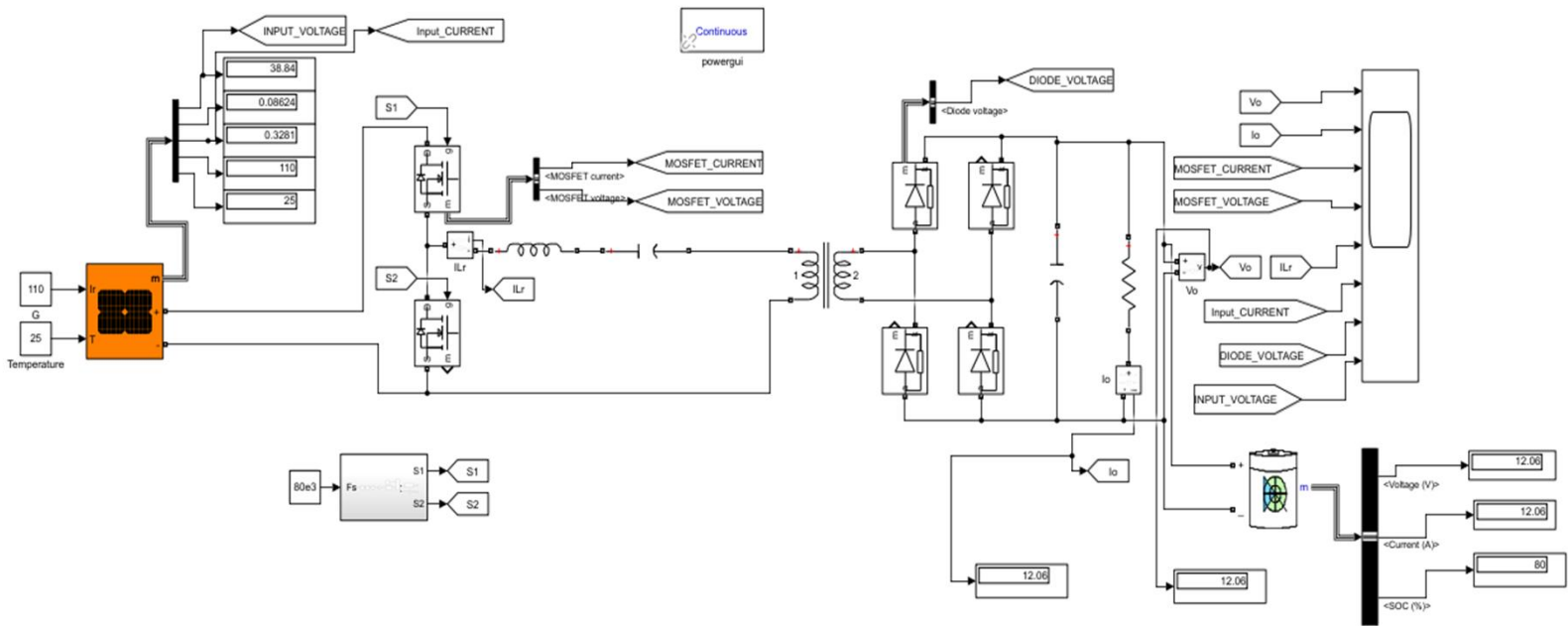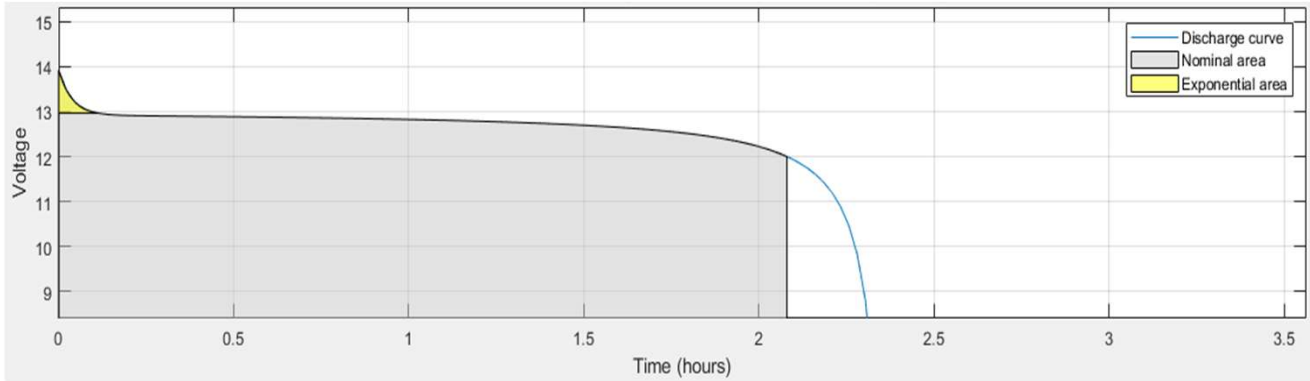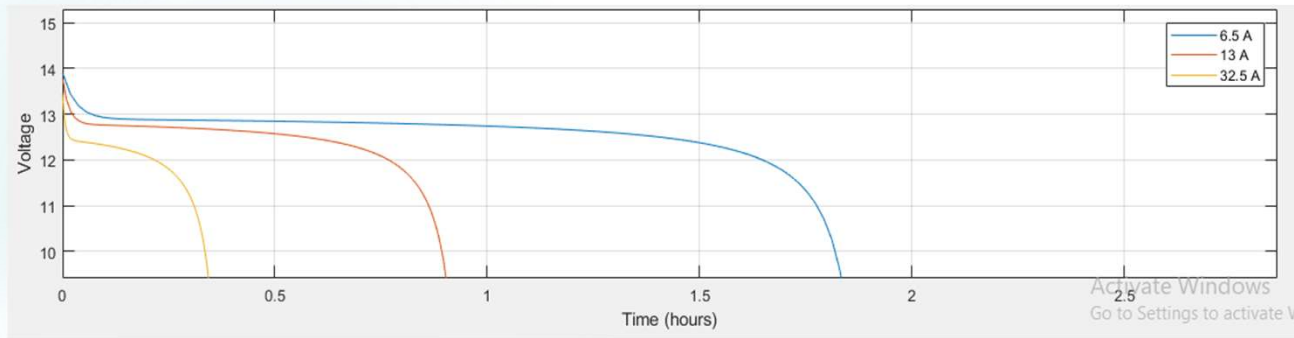

Fig 7.19: Matlab simulation for open loop LC resonant converter for battery charging application.

Table 12: Different parameters

Parameters	values
Vin	35V
f_o	200Khz
Ro	6.15Ω
L	12.733µH
C	49.73µF
Io	12A
Vo	12V
Po	144W

30-03-2023

Fig 28: Nominal current discharge characteristics of the battery.

Fig 29: Voltage vs Time characteristics of Lithium-Ion battery.

Table 13: Lithium-Ion battery parameters

Parameters	Ratings
Nominal voltage (V)	12V
Rated capacity (Ah)	12Ah
Initial state of charge (%)	80%
Battery response time (s)	1s
Maximum capacity (Ah)	12Ah
Cut off voltage (V)	9V
Fully charged voltage (V)	13.9678V
Nominal discharge current (A)	5.2174A
Internal resistance (Ohms)	0.01 Ohms
Capacity (Ah) at nominal voltage	10.8522Ah

30-03-2023
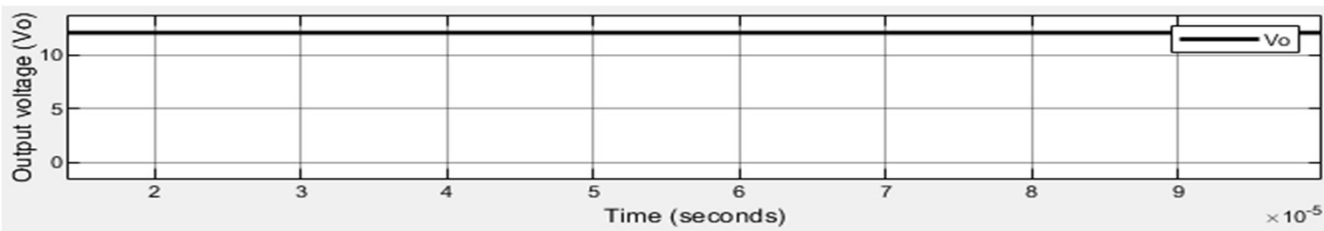
Fig 30: Output voltage of series resonant converter for battery charging under open loop.
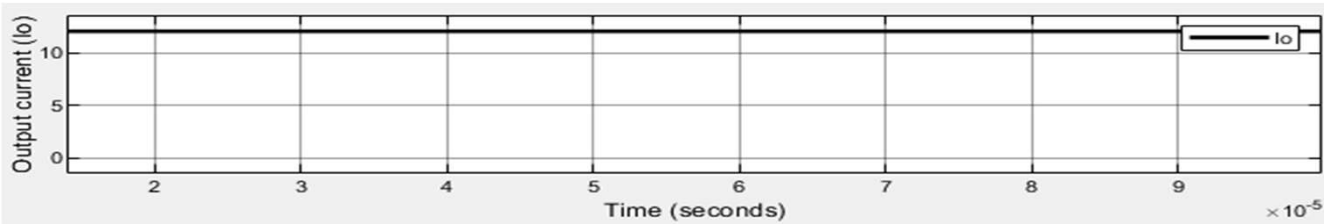
Fig 31: Output current of series resonant converter for battery charging under open loop
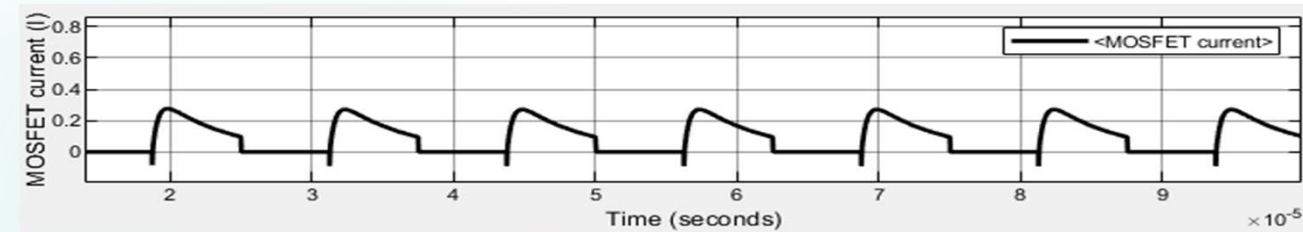
Fig 32: mosfet current of series resonant converter for battery charging under open loop

Fig 33: mosfet voltage of series resonant converter for battery charging under open loop

Fig 34: Inductor current of series resonant converter for battery charging under open loop

Fig 35: Input current of series resonant converter for battery charging under open loop

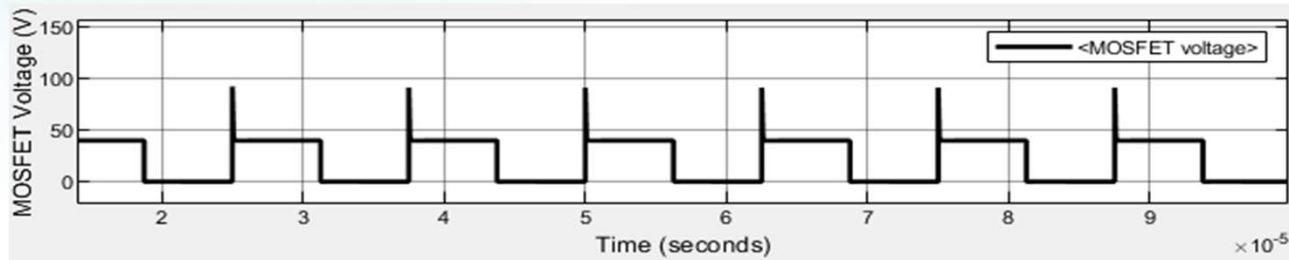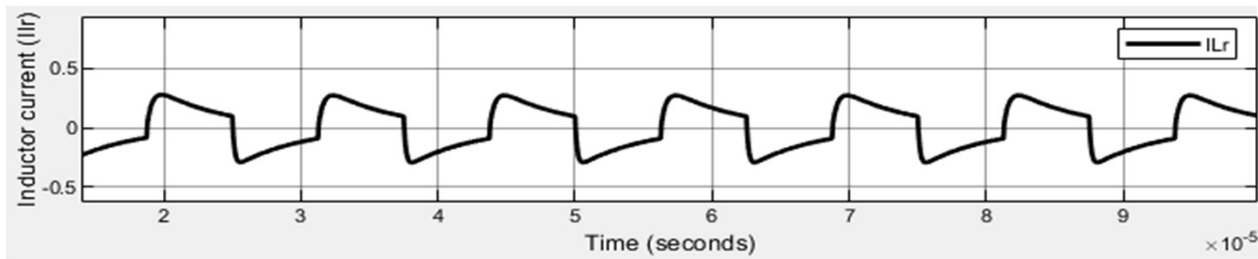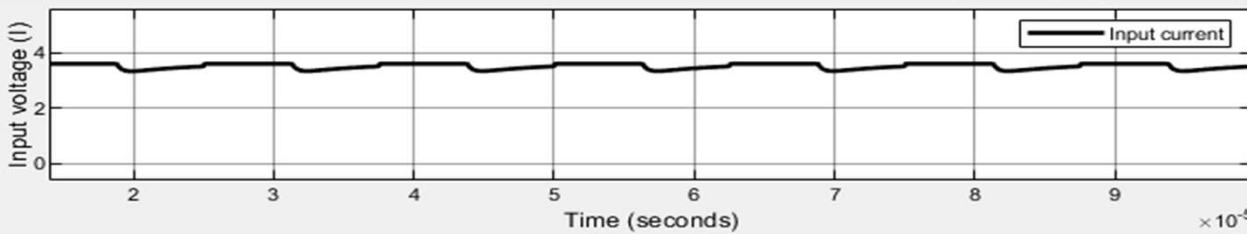
Fig 36: Diode voltage of series resonant converter for battery charging under open loop

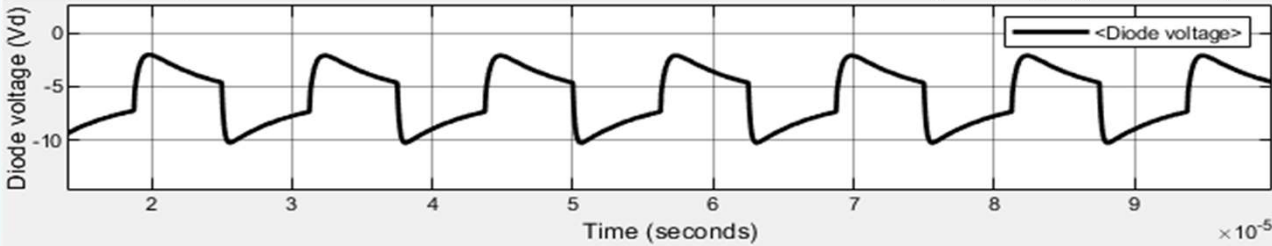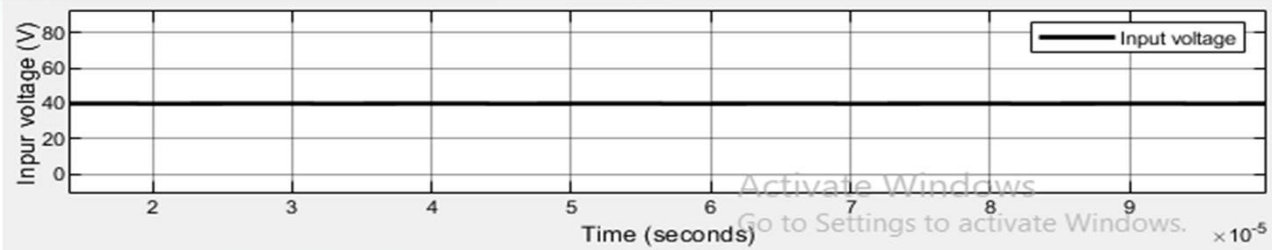**Fig 37: Input voltage of series resonant converter for battery charging under open loop**

64

Closed Loop Matlab Programming for Average Current Mode Control of Series Resonant Converter.

```matlab
clc;
clear all;
close all;
%% Avergae Current Mode
Controller Design for LC Resonant
Converter

%% LC series resonant converter
- Hard ware Specification
Ls = 12.73e-6;
Cs = 49.73e-9;

Cf = (5*330e-6 + 40e-06);
rd = 0.00725+0.008;


rc = 15e-3/6;
rs = 15e-3;
n = 2;

%% LC Operating Point
Duty = 0.5;
Vin = 40;
Po_desired = 150;
Vo = 12;
Io = Po_desired/Vo;
R = Vo/Io;
Re = (8*(n^2)/(pi^2))*(rd+R);

%% Sensor Circuit Parameters
% Current sensor parameters
Rfc = 10;
Cfc = 2e-6 ;
Gct = 1/50;
Gopamp = (1+(576/300));
```

```matlab
Gpd = 20;
Gavg = 2/pi;

% Voltage sensor parameters
R9 = 1.50e3 ;
R8 = 5.02e3 ;
Cfv = 2000e-12;


%% ADC and PWM module gains
Gpwm = 1;
Kadc = 3.33 ;


%% Enter controller design parameters
for desired controller
fci = 5540;


fcv = 1130;


TsC = 1/200000;


TsV = 1/50000;


Delay_Total = 3.558e-06;
T_zoh1 = TsV;
T_zoh2 = TsC;


% Inner loop controller parameters need
to be adjusted for desired PM (See Plot-2
to adjust PM of inner loop-gain)
z1shift = 0.6661;
z2shift = 0.3737;
p1shift = 0.06132;


% Outer loop controller parameter
```

```matlab
need to be adjusted for desired PM (see Plot-3 to
adjust PM of outer loop-gain)
Wv = 2500;

%% Finding switching frequency based on Gain-
Frequency Curve
Vq = (Vin/2);              % Half-bridge voltage

W0 = 1/sqrt(Ls*Cs) ;
f0 = W0/(2*pi);

Qfac = sqrt(Ls/Cs)/Re;
GainR = n*(Vo+(rd*Io))/Vq;

% Finding ratio of switching frequency to
resonance frequency
Aa = (Qfac^2);
Bb = (2*(Qfac^2));
Cc = ((Qfac^2));
Dd = 1;
Fxp = [Aa 0 Bb 0 Cc 0 Dd];
Fxr = roots(Fxp);
Fxreal = real(Fxr);
Fx = max(Fxreal);
fs = Fx*f0;
Ws = 2*pi*fs;

%% Sampling time and Digital Delay Transfer
Function
s=tf('s');

% 1st Order Pade's Approximation for delays
H_outDelay=(1-
s*(Delay_Total/2))/(1+s*(Delay_Total/2));
```

```matlab
% Zero order hold due to out loop
lower sampling rate
exp_Ts_coeff = s*T_zoh1/2;
exp_Ts1 = (1-
exp_Ts_coeff+exp_Ts_coeff^2-
exp_Ts_coeff^3)/(1+exp_Ts_coeff+exp_
Ts_coeff^2+exp_Ts_coeff^3);

H_zoh1 = minreal((1 -
exp_Ts1)/(s*T_zoh1));


exp_Ts_coeff = s*T_zoh2/2;
exp_Ts2 = (1-
exp_Ts_coeff+exp_Ts_coeff^2-
exp_Ts_coeff^3)/(1+exp_Ts_coeff+exp_
Ts_coeff^2+exp_Ts_coeff^3);


H_zoh2 = minreal((1 -
exp_Ts2)/(s*T_zoh2));


%% Steady-State parameters; Derived
in the application note
Ves = (2*Vin/pi);

X = [ rs+Re  Ls*Ws  1    0    -Re   0
;
  -Ls*Ws  rs+Re   0    1    0    -Re  ;
   1    0    0    -Cs*Ws  0    0   ;
   0    1    Cs*Ws  0    0    0   ;
   Re   0    0    0    -Re   Ws ;
```

```matlab
 0   Re   0   0    Ws  -Re  ] ;

U0 = [ Ves ; 0 ; 0 ; 0; 0 ; 0 ];

Y = linsolve(X,U0) ;

Is = Y(1); Ic = Y(2) ; Vs = Y(3) ; Vc = Y(4) ;
Ims = Y(5) ; Imc = Y(6) ;

Ipc = Ic-Imc;

Ips = Is-Ims ;

Ipp = sqrt(Ips^2+Ipc^2);

Ir = sqrt(Is^2+Ic^2);

Im = sqrt(Ims^2+Imc^2);

Isp = n*Ipp ;

Vcf = 2*Isp*R/pi;

%%% Small-Signal coefficients; Derived in
the application note

rc1 = R*rc/(R+rc);

Hip =
((4*n*rc1*Vcf*Ipc^2)/(pi*rc*Ipp^3))+((8*(
rd+rc1)*n^2)/(pi^2));

Hic = -
(4*n*rc1*Vcf*Ips*Ipc)/(pi*rc*Ipp^3);

Hvcf = (4*n*rc1*Ips)/(pi*rc*Ipp);

Gip = -
(4*n*rc1*Vcf*Ips*Ipc)/(pi*rc*Ipp^3);

Gic =
((4*n*rc1*Vcf*Ips^2)/(pi*rc*Ipp^3))+((8*(
rd+rc1)*n^2)/(pi^2));
```

```matlab
Gvcf = (4*n*rc1*Ipc)/(pi*rc*Ipp);


Kis = (2*n*Ips)/(pi*Ipp);

Kic = (2*n*Ipc)/(pi*Ipp);


Js= (2/pi)*Is/sqrt(Is^2+Ic^2);

Jc= (2/pi)*Ic/sqrt(Is^2+Ic^2);


%%% LC EDF Model system matrices
A = [ -((Hip+rs)/Ls)   -(Ws+(Hic/Ls)) -
1/Ls  0  (Hip/Ls)    (Hic/Ls)     -
(Hvcf/Ls)  ;

  (Ws-(Gip/Ls))   -((Gic+rs)/Ls)  0    -
1/Ls  (Gip/Ls)    (Gic/Ls)     -
(Gvcf/Ls)  ;

  1/Cs     0      0     -Ws  0      0
0    ;

   0     1/Cs   Ws   0  0      0
0    ;

  (Hip)    (Hic)   0   0  -(Hip)    -
(Ws+(Hic))   (Hvcf)  ;

  (Gip)    (Gic)   0   0  (Ws-(Gip))
-(Gic)    (Gvcf)  ;

  ((Kis*rc1)/(Cf*rc)) ((Kic*rc1)/(Cf*rc))
0   0  -((Kis*rc1)/(Cf*rc)) -
((Kic*rc1)/(Cf*rc))  -rc1/(R*Cf*rc) ];
```

```matlab
B = [ -Ic*W0   ;
  Is*W0   ;
  -Vc*W0   ;
  Vs*W0   ;
  -Imc*W0   ;
  Ims*W0   ;
  0   ] ;

C= [ Kis*rc1  Kic*rc1  0  0  -Kis*rc1   -Kic*rc1
rc1/(rc)   ;
  Js    Jc   0  0  0     0   0     ];

D = [ 0 ;
  0 ];

%%% EDF model transfer function
sys = ss(A,B,C,D);
EDF = tf(sys);

Gvw = EDF(1);
Giw = EDF(2);

P = pole(Giw);
[N,K] = zero(Giw);
Giw = minreal(zpk(N,P,K));

figure(1);
P = bodeoptions;
P.Grid = 'on';
P.FreqUnits = 'Hz';
P.PhaseWrapping = 'off' ;
bode(Giw,P); hold on;

%%% Current sensor gain
Gif =1/(Rfc*Cfc*s+1);
Gisense = Gif*Gct*Gopamp*Gpd/Kadc;
```

```matlab
%%% Current Loop Compensator
design (2P2Z)
% Chosen Gain Crossover frequency
% Compensator one pole is to cancel
the effect of Wesr.
% place the compensator two zeros at
complex pole location to cancel the
effect of of complex zeros
% and get the proper shape of open-
loop transfer function
wc = 2*pi*fci ;

%poles of plant and sensor gain
[Niw,Kiw] = zero(-Giw*Gisense);
Piw = pole(-Giw*Gisense);

Piw = Piw( Piw<=0 );
Niw = Niw( Niw<=0 );

Nreal = real(Niw);
Preal = real(Piw);

[Nmax,Index_N] = max(Nreal);
[Pmax,Index_P] = max(Preal);

% Compensator poles-zeros selection
Wesr = Nreal(Index_N);

Wz1 = Preal(Index_P)/z1shift;
```

66

```matlab
Wz2 = Preal(Index_P)/z2shift;
Wp1 = Wesr/p1shift ;

Gci = (s-Wz1)*(s-Wz2)/(s*(s-Wp1));

% Plant Gain calculation at Crossover
frequency :
[Giw_fc Phiw_fc] = bode(-
Giw*Gisense,wc);

%Compensator gain calculation at
cross-over frequency
[Gci_fc Phci_fc] = bode(Gci,wc);

% At Crossover frequency K*Gc*Gp =
1
Kc = 1/(Giw_fc*Gci_fc);
% Overall compensator transfer
function
Gci = Kc*Gci ;

% Discretization of compensator
transfer function using tustin or bi-
linear transfomation
Gci_d = c2d(Gci,TsC,'tustin') ;

% Current-Loop-gain calculation
Giol = minreal(-Giw*Gisense*Gci) ;

figure(2);
P = bodeoptions;
P.Grid = 'on';
```

```matlab
P.FreqUnits = 'Hz';
P.PhaseWrapping = 'off';
bode(Giol, P); hold on;
margin(Giol);

%% Closed-Loop Transfer function
(Current Loop)
Gcl = (-
Gci*Giw*H_outDelay*Gpwm)/(1-
(Gisense*Gci*H_outDelay*H_zoh2*Giw
*Gpwm));
% Gcl = (-Gci*Giw*Gpwm)/(1-
(Gisense*Gci*Giw*Gpwm));

%% feedback or sensor circuit gain
Gp_sensor = R9/(R9+R8);
Rfv = R8*R9/(R8+R9);
Gpfc = Gp_sensor/(Rfv*Cfv*s+1);
Gfv = Gpfc/Kadc ;

%% Voltage-to-Current Transfer
function
Giv = -Gvw/-Giw ;

%% Current Loop Compensator design
(PI)
w_cv = 2*pi*fcv;
Gvl = Gcl*Giv*Gfv;

Gcv =(s+Wv)/s ;

% Compensator gain calculation at
cross-over frequency
```

```matlab
[Gcv_fcv phic_fcv] = bode(Gcv,w_cv) ;

% Plant Gain calculation at Crossover
frequency :
[Gvl_fcv phi_fcv] = bode(Gvl,w_cv);

% At Crossover frequency
K*Gc*Gp*G_sensor = 1 :
Kc = 1/(Gvl_fcv*Gcv_fcv);

% Overall compensator transfer function
Gcv = Kc*Gcv ;

Gcv_d = c2d(Gcv,TsV,'tustin') ;
Gvs = Gcv*Gvl*H_zoh1*H_outDelay;

figure(3);
P = bodeoptions;
P.Grid = 'on';
P.FreqUnits = 'Hz';
P.PhaseWrapping = 'off' ;
bode(Gvs, P); hold on;
margin(Gvs);

%% Voltage to Frequency factor for
simulink model
Vab = 40/2   ;
ws = 2*pi*fs   ;
Xr = ws*Ls   ;
Xm = ws   ;
XC = 1/(ws*Cs)  ;
p = (Xr - XC + Xm)/Xm;
fr = 200e3    ;

frequencytovoltagefactor =
(2*pi^2*fr^3*Cs)/Vab/p^2 ;
```
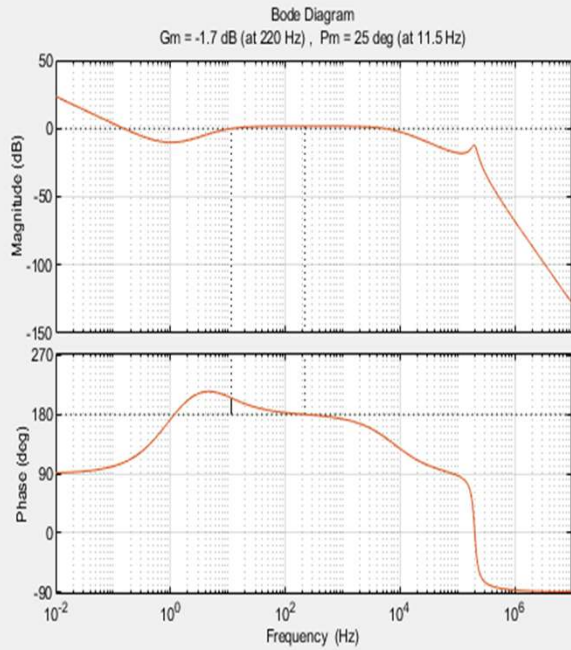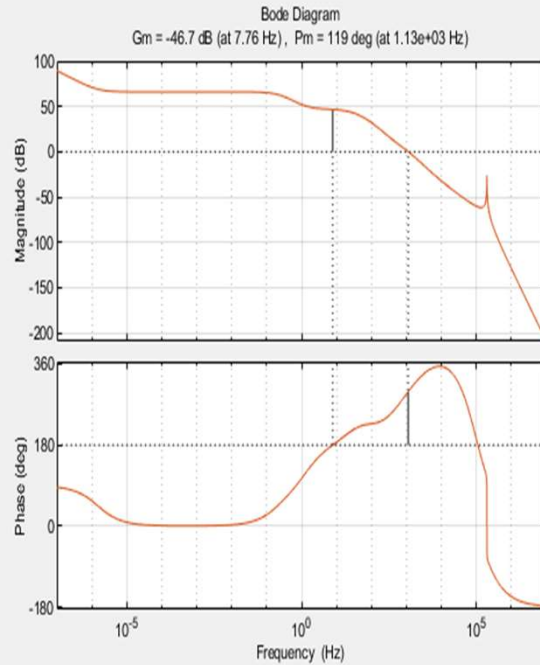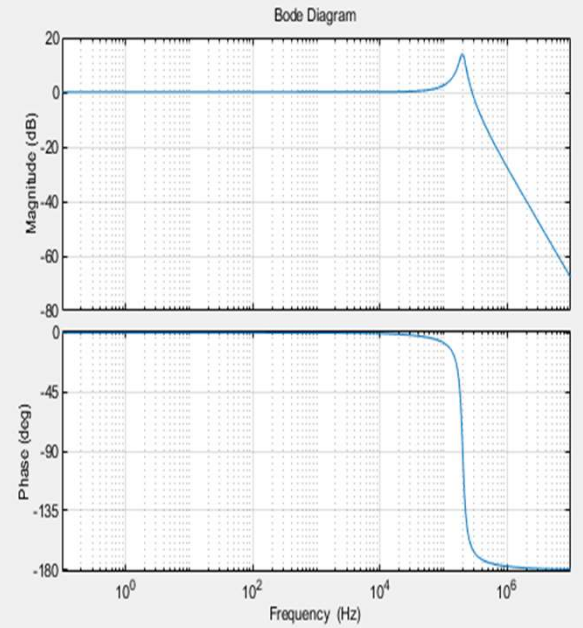
Fig 38: Bode plot of Current-Loop-gain for closed loop LC resonant converter

Fig 39: Bode plot of Outer loop-gain for closed loop LC resonant converter.

Fig 40: Bode plot for LC converter frequency to output voltage transfer function for closed loop

11. CONCLUSION

- A Half-Bridge LC resonant converter is designed and simulated under various frequencies, at resonance frequency, above resonance frequency and below resonance frequency.

- It has obtained that the LC resonant converter gives it better performance near the resonance frequency.

- PV system is used to provide supply to the LC resonant converter, it is designed to provide 35V, 40V and 45V under temperature of 45C, 25C and 15C.The analysis of LC resonant converter is done for Continuous and Discontinuous mode of operations. The supply of 35V, 40V and 45V is bucked to 12V which is used for battery charging.

30-03-2023

- **The design of resonant tank is done for line regulation, load regulation, and efficiency. Detailed design and selection of Mosfet, Inductor, Capacitor, Transformer, Rectifier circuit, Filter circuit and Load design is done.**

- **The mathematical modeling for the resonant converter is carried out by First Harmonic Approximation (FHA) and Small signal modeling for series resonant converter.**

- **For a closed loop analysis the controller used here is Average Current Mode Controller (ACMC) which is a combination of voltage and current mode controller and it is found that ACMC has various advantages over them.**

REFERENCES

[1] Fahad Alaql1 and Issa Batarseh "Review and Comparison of Resonant DC-DC Converters for Wide-Output Voltage Range Applications" in IEEE Transactions on Power Electronics, vol. 31, no. 3, pp. 2596–2608, 2020

[2] H. Afshang and F. Tahami " Voltage Regulation of DC-DC Series Resonant Converter Operating in Discontinuous Conduction Mode: The Hybrid Control Approach" IJE TRANSACTIONS B: Applications Vol. 32, No. 11, (November 2019) 1610-1619

[3] Mehdi Mohammadi and Martin Ordonez "Fast Transient Response of Series Resonant Converters Using Average Geometric Control" IEEE Trans. on Power Electron., Vol. 30, no. 8, pp. 4560-4572, Aug. 2019.

[4] Federico Martin Ibanez, Jose Martin Echeverria, Javier Vadillo, Luis Fontan CEIT and Manuel de Lardizabal "A step-up bidirectional series resonant DC/DC converter using a continuous current mode" in IEEE Transactions on Power Electronics, vol.14, no.1, pp.15,24, Jan 2021.

[5] Swati Tandon and Akshay Kumar Rathore " Novel Series LC Resonance-Pulse Based ZCS Current-Fed Full-Bridge DC-DC Converter: Analysis, Design and Experimental Results" in IEEE Transactions on Power Electronics, vol. 25, no. 3, pp. 686-698, March 2020.

[6] Song Hu, Xiaodong Li and Ashoka K.S. Bhat "Operation of a Bidirectional Series Resonant Converter with Minimized Tank Current and Wide ZVS Range" in IEEE Trans. Power Electron., vol. 30, no. 12, pp. 6488-6494, Dec. 2018.

[7] B. Zhao, Q. Song, W. Liu, G. Liu, and Y. Zhao, "Universal high-frequency-link characterization and practical fundamentaloptimal strategy for dual-active-bridge DC-DC converter under PWM plus phase-shift control," IEEE Trans. Power Electron., vol. 30, no. 12, pp. 6488-6494, Dec. 2018.

[8] Y. W. Cho, W. J. Cha, J. M. Kwon, and B. H. Kwon, "Highefficiency bidirectional DAB inverter using a novel hybrid modulation for stand-alone power generating system with low input voltage," IEEE Trans. Power Electron, vol. 31, no. 6, pp. 4138- 4147, Jun. 2019.

30-03-2023

71

[9] A. Tong, L. Hang, and S. Gao, "Modeling and analysis of dualactive-bridge isolated bidirectional DC/DC converter to minimize RMS current with whole operating range," IEEE Trans. Power Electron., vol. 33, no. 6, pp. 5302-5316, Jun. 2020.

[10] B. Zhao, Q. Yu, and W. Sun, "Extended-phase-shift control of isolated bidirectional DC–DC converter for power distribution in microgrid," IEEE Trans. Power Electron., vol. 27, no. 11, pp. 4667-4680, Nov. 2021.

[11] X. Liu, Z. Q. Zhu, D. A. Stone, M. P. Foster, W. Q. Chu, I. Urquhart, and J. Greenough, "Novel dual-phase-shift control with bidirectional inner phase shifts for a dual-active-bridge converter having low surge current and stable power control," IEEE Trans. Power Electron., vol. 32, no. 5, pp. 4095-4106, May 2020.

[12] S. S. Muthuraj, V. K. Kanakesh, P. Das, and S. K. Panda, "Triple phase shift control of an LLL tank based bidirectional dual active bridge converter," IEEE Trans. Power Electron., vol. 32, no. 10, pp. 8035-8053, Oct. 2019.

[13] F. Musavi, M. Craciun, D. S. Gautam, W. Eberle, and W. G. Dunford, "An LLC resonant DC–DC converter for wide output voltage range battery charging applications," IEEE Trans. Power Electron., vol. 28, no. 12, pp. 5437-5445, Dec. 2018.

[14] F. Musavi, M. Craciun, D. S. Gautam, and W. Eberle, "Control strategies for wide output voltage range LLC resonant DC–DC converters in battery chargers," IEEE Trans. Veh. Technol., vol. 63, no. 3, pp. 1117-1125, Mar. 2017.

[15] J. H. Jung, H. S. Kim, M. H. Ryu, and J. W. Baek, "Design methodology of bidirectional CLLC resonant converter for highfrequency isolation of DC distribution systems," IEEE Trans. Power Electron., vol. 28, no. 4, pp. 1741-1755, Apr. 2018.

[16] Z. U. Zahid, Z. M. Dalala, R. Chen, B. Chen, and J. S. Lai, "Design of bidirectional DC–DC resonant converter for vehicleto-grid (V2G) applications," IEEE Trans. Transport. Electrific, vol. 1, no. 3, pp. 232-244, Oct. 2019.

THANK YOU